



LkH α 225 (V1318 Cyg) South in Outburst

Lynne A. Hillenbrand¹, Howard Isaacson^{2,3} , Antonio C. Rodriguez^{1,4} , Michael Connelley⁵ , Bo Reipurth⁵ ,Michael A. Kuhn¹ , Tracy Beck⁶ , and Diego Rodriguez Perez⁷¹ Department of Astronomy, California Institute of Technology, Pasadena, CA 91125, USA; lah@astro.caltech.edu² Astronomy Department, University of California, Berkeley, CA 94720, USA³ University of Southern Queensland, Toowoomba, QLD 4350, Australia⁴ Department of Physics, Stanford University, Palo Alto, CA 94305-4013, USA⁵ Institute for Astronomy, University of Hawaii at Manoa, 640 N. Aohoku Place, Hilo, HI 96720, USA⁶ Space Telescope Science Institute, 3700 San Martin Drive, Baltimore, MD 21218, USA⁷ Guadarrama Observatory, MPC458, Madrid, Spain

Received 2020 November 17; revised 2021 December 28; accepted 2021 December 29; published 2022 February 7

Abstract

Magakian et al. called attention to the current bright state of LkH α 225 South, a well-known highly embedded, intermediate-mass young stellar object that over the past two decades has brightened visually from $>20^m$ to $<13^m$. We present recent optical photometric monitoring showing colorless, nonsinusoidal, periodic brightness oscillations occurring every 43 days with amplitude ~ 0.7 mag. We also present new flux-calibrated optical and near-infrared spectroscopy, which we model in terms of a Keplerian accretion disk, and high-dispersion spectra that demonstrate similarity to some categories of “mixed-temperature” accretion-outburst objects. At blue wavelengths, LkH α 225 South has a pure absorption spectrum and is a good spectral match to the FU Ori stars V1515 Cyg and V1057 Cyg. At red optical and infrared wavelengths, however, the spectrum is more similar to Gaia 19ajj, showing emission in TiO, CO, and metals. Sr II absorption indicates a low-surface-gravity atmosphere. There are also signatures of a strong wind/outflow. LkH α 225 South was moderately bright in the early 1950s as well as in the late 1980s, with evidence for deep fades during intervening epochs. The body of evidence suggests that LkH α 225 South is another case of a source with episodically enhanced accretion that causes brightening by orders of magnitude, and development of a hot absorption spectrum and warm wind. It is similar to Gaia 19ajj, but also reminiscent in its long brightening time and brightness oscillation near peak to the embedded sources L1634 IRS7 and ESO Ha 99.

Unified Astronomy Thesaurus concepts: [Young stellar objects \(1834\)](#); [FU Orionis stars \(553\)](#); [Circumstellar disks \(235\)](#); [Protoplanetary disks \(1300\)](#); [Stellar accretion disks \(1579\)](#)

1. Introduction

The young stellar object LkH α 225 South (also designated V1318 Cyg South) is located at 20:20:30.59 +41:21:26.3 (J2000) and is associated with a small cluster of young stars usually identified as the BD+40° 4124 cluster. The two nebulous early-type emission-line stars BD+40° 4124 (V1685 Cyg) and LkH α 224 (V1686 Cyg) that define the optical appearance of the cluster (see Figure 1) are long-recognized—and, in fact, original—Herbig Ae/Be stars (Herbig 1960). But it is LkH α 225 South that is the dominant source in mid-infrared, far-infrared, and millimeter maps (e.g., Aspin et al. 1994; see also Spitzer and WISE images). The distance to the region is approximately 900 pc.

Historically, LkH α 225 has been considered a potential wide binary, with a north–south pair separated by about 5" and an adjoining ridge of dense nebulosity. Both the northern and southern sources have protostellar Class I-type spectral energy distributions (SEDs).

LkH α 225 South is generally touted as the source responsible for much of the star formation “activity” in the overall region, and is one of its more well-studied objects. In addition to being the brightest source locally at mid-infrared wavelengths, LkH α 225 South has strong millimeter

continuum. Indeed, it is well known in the massive star, star formation community as a deeply embedded, moderate-luminosity protostellar object that drives a multicomponent, massive bipolar outflow.

Outflowing gas was first indicated in the spectrum of Andrillat & Swings (1976) via strong absorption in the He I 10830 Å line, consistent with a wind, along with strong emission in the Ca II triplet lines. Magakian & Movsessian (1997) reported on a spectrum from 1978 with H α described as “rather intense and possibly [with] a P Cyg profile” and Na D as “distinct”. Shocked H $_2$ gas in the near-infrared was first detected by Aspin et al. (1994) and later mapped by Navarete et al. (2015, their Figure A90). van den Ancker et al. (2000) studied mid-infrared H $_2$ and also presented forbidden line-emission maps. Sandell et al. (2012) detected the outflow in higher-spatial-resolution [C II] profiles. The molecular outflow was investigated in low-J CO by Palla et al. (1995) and Matthews et al. (2007), and in high-J CO by Sandell et al. (2012). The ionized jet was mapped at radio wavelengths by Purser et al. (2021, their Figure B15), who found alignment with the H $_2$ lobes of Navarete et al. (2015) and calculated a bolometric luminosity six times that of nearby BD+40° 4124, which, adjusting to the distance we adopt, amounts to nearly 2600 L_{\odot} .

Palla et al. (1995) reported H $_2$ O maser emission. Marvel (2005) further characterized the maser spot distribution and postulated that two outflow sources are involved. Looney et al. (2006) recognized that the maser position is offset to the



Original content from this work may be used under the terms of the [Creative Commons Attribution 4.0 licence](#). Any further distribution of this work must maintain attribution to the author(s) and the title of the work, journal citation and DOI.

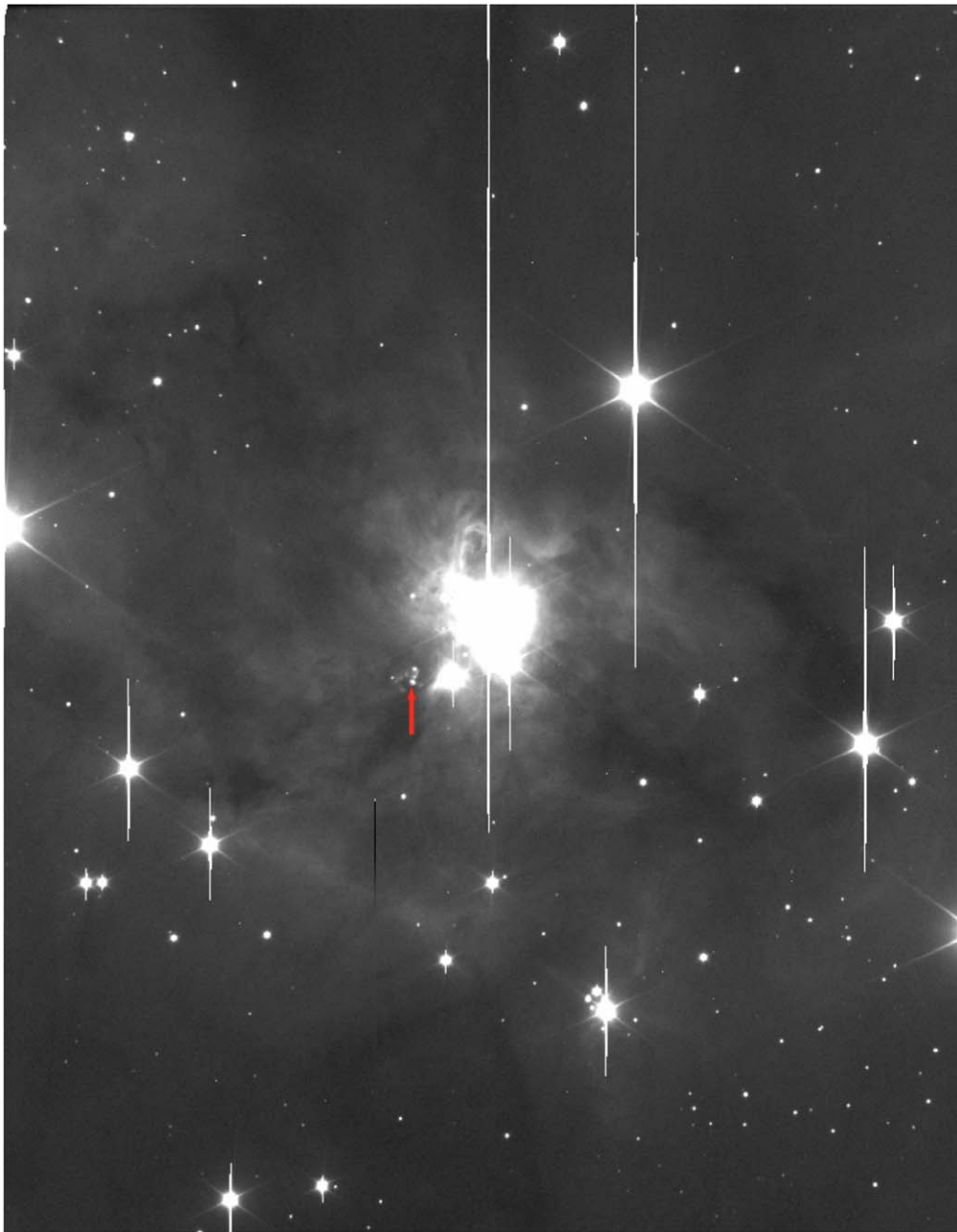


Figure 1. 1999 Keck/LRIS R -band image ($\sim 6' \times 8'$) with orientation north upwards and east to the left. Bright nebulosity is associated with both BD+40° 4124 (center) and V1686 Cyg (southeast of center). The LkH α 225 North–South pair are due east of V1686 Cyg. At this epoch, LkH α 225 South (indicated by red arrow) was in a prolonged faint state (see Figure 3).

northeast from LkH α 225 South, and demonstrated its coincidence with an extended 3.1 mm continuum source, suggesting that there may be yet another embedded protostellar source at this position. Bae et al. (2011) reported methanol maser emission in the area. The potential for spatial confusion seems to render unclear the origin of the large-scale outflow, and whether it is LkH α 225 South, as often advocated, or the embedded millimeter source that is coincident with the masers.

There is also significant uncertainty about the mass of LkH α 225 South. It is assumed to be intermediate-to-high mass, based on the integrated luminosity in the SED, with $1600 L_{\odot}$ derived by Aspin et al. (1994). A spectral type of Ae-Fe was declared by Hillenbrand et al. (1995) for each of the two components of LkH α 225, but this assessment was from a rather low signal-to-

noise (S/N) spectrum with little in the way of absorption lines. Then there is the spectral type of A4Ve reported by the SIMBAD database, attributed to Mora et al. (2001); this is clearly a typographical error, as the cited paper does not contain LkH α 225, only the nearby LkH α 224 (V1686 Cyg), which is indeed listed as A4Ve by Mora et al. (2001). Furthermore, the observations in the paper were taken in 1998 when LkH α 225 was faint (as discussed below) and thus unlikely to have been a successful spectroscopic target. We make independent progress on a mass estimate in the context of SED fitting (Section 7), though do not fare much better in constraining M_{*} than the loose estimates already made from observations.

There are a total of three young stellar objects in the BD +40° 4124 cluster having the characteristics of intermediate-

mass, pre-main-sequence stars, all located within a small molecular core region only ~ 0.2 pc in size. An accompanying population of lower mass T Tauri-type objects is present, as well, but the region is unusual in its high percentage of intermediate-mass stars relative to the subsolar mass population (Hillenbrand et al. 1995).

Our interest in this region was piqued again when Magakian et al. (2019) reported a slowly developing outburst in LkH α 225 South, finding that the current bright state was reached in 2015. These authors recount the variability history of the source and illustrate recent spectra showing a mix of absorption and emission lines, plus evidence for outflowing gas.

In the current paper, we conduct an extensive investigation of the current bright state of the enigmatic source LkH α 225 South. Figure 2 shows a recent guider camera image from late 2020. We report new photometric monitoring from Palomar/P48/the Zwicky Transient Facility (ZTF) that indicates an oscillatory nature to the bright state. We also present Palomar/P200/Double Spectrograph (DBSP) and Keck/High Resolution Echelle Spectrometer (HIRES) optical spectroscopy, and Infrared Telescope Facility (IRTF)/SpeX and Keck/Near Infrared Spectrometer (NIRSPEC) infrared spectroscopy, all showing strong accretion and outflow signatures. Given its historically faint state, we have not previously had the opportunity to perform a good-quality optical photometric and spectroscopic study of LkH α 225 South. We also assemble the long-term light curve of the source, and present previously unpublished imaging and spectroscopy from the faint state as further context. Finally, we model LkH α 225 South as an accretion-disk-dominated system, quantifying the outburst-accretion rate and the stellar parameters.

2. Historical Light Curve of LkH α 225 South

Figure 3 illustrates the light curve that can be assembled for LkH α 225 South over the past 35 yr, including photometry newly reported here, which is highlighted in Figure 4.

The observed brightness in several different red optical filters has been converted to an equivalent r -band magnitude for plotting purposes. At epochs earlier than those shown in the figure, the variability of the LkH α 225 system was well documented during the 1950s–1970s, as discussed also in detail by Magakian et al. (2019), but the variations were not well quantified in the literature. Furthermore, due to the small separation ($\sim 5''$) of the north–south pair, the intervening ridge of nebular material, and the likely variability of *each* of the two components, there can be confusion in interpreting the older photometry. However, the evidence does seem to suggest irregular variations of at least several magnitudes in LkH α 225 South. While the typical photographic magnitude brightness was 17–18^m, two “eruptions” to approximately 15.5^m were documented by Wenzel (1972). LkH α 225 South can be seen in all available plate data from the 1960s as the brighter of the north–south pair (e.g., DSS1, Herbig 1960; Strom et al. 1972). However, the source is somewhat fainter in DSS2 images.

Later, in the 1980s, the LkH α 225 system was monitored more systematically, and magnitudes were reported in known photometric systems. Typically the brightness measurements were below 16^m visually. Ibragimov et al. (1988) reported large color variations of several magnitudes. Shevchenko et al. (1993) reported V -band variations between 15 and 19^m over JD = 2446345 and 2448159. Seemingly inconsistent with the other measurements from this era, Terranegra et al. (1994)

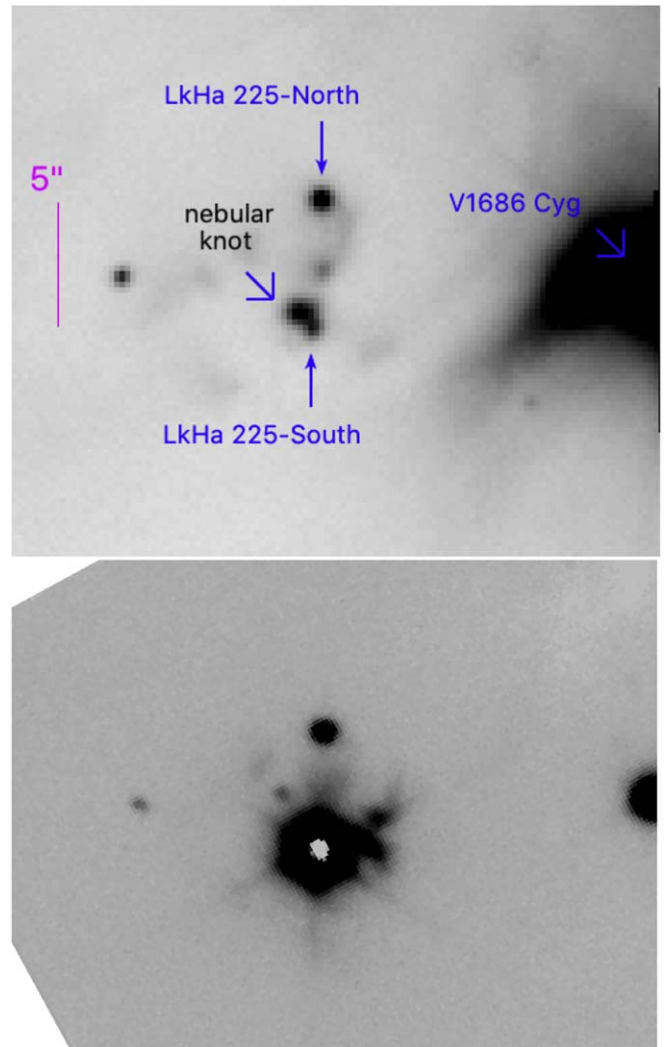


Figure 2. Top panel: expanded view of the faint-state 1999 R_c -band image of Figure 1, centered here on the LkH α 225 system, with LkH α 225 North and LkH α 225 South both marked. The well-known ridge of nebulosity between them is faint in this stretch, but can be seen extending from North southward to a nebular knot. An even brighter nebular knot along the same line, about $0.8''$ northeast (PA = 35.5°) of LkH α 225 South, is marked. The position appears to be coincident with maser spots and 3.1 mm continuum emission; see text. The knot is brighter than LkH α 225 South itself at this particular epoch, and it has some east–west extension. At the western edge of the image, the extended bright nebulosity is associated with V1686 Cyg (LkH α 224) which is just off frame. Bottom panel: bright-state Y -band image taken in 2020 with Keck/NIRSPEC-SCAM; white pixels indicate saturation in the individual 0.655 sec exposures. The frame stack comprises 30 seconds of total integration. Relative to the earlier image above, LkH α 225 South has brightened dramatically compared to LkH α 225 North. A faint instrumental ghost appears to the northeast of LkH α 225 South; this is not the same position as the nebular source marked in the top panel.

reported $V = 13.5^m$ along with Strömgren system photometry indicating a mid-B spectral type; these data were taken in either⁸ 1988 September or 1990 June, and are several magnitudes brighter than the data given in Shevchenko et al. (1993). We disregard them in what follows, suspecting they may be observations of LkH α 224 (V1686 Cyg) just to the west, rather than of LkH α 225. As discussed above, the same

⁸ The observation dates and the objects are specified, but the correspondence between them is unspecified.

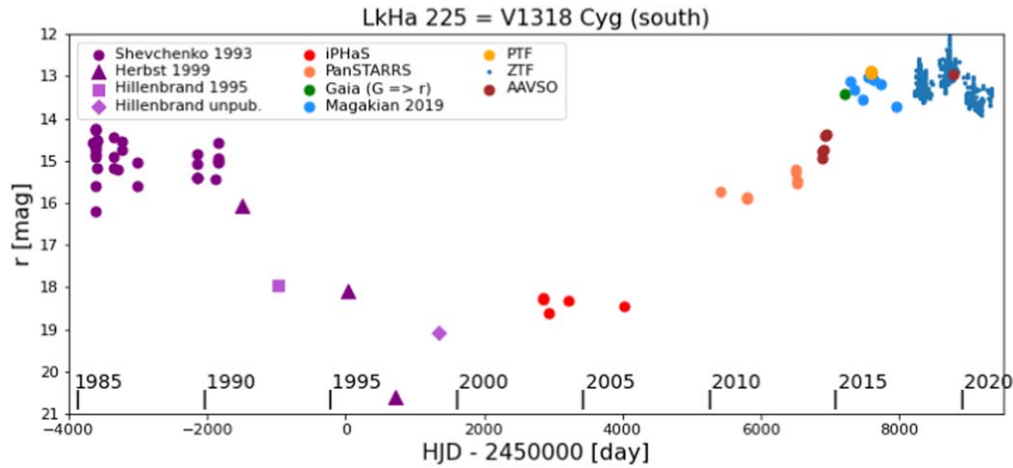


Figure 3. Light curve for LkH α 225 South from the 1980s to the present, demonstrating the gradual fade over about 15 yr and subsequent rise by >6 mag over the next 20 yr. The published R -band data have been transformed to r using an advertised transformation equation (<http://www.sdss3.org/dr8/algorithms/sdssUBVRITransform.php#Lupton2005>), with the correction here typically a shift by 0.6 mag fainter. The PanSTARRS and ZTF photometry has been converted from native AB to Vega magnitudes. The Gaia DR2 G -band photometry has been corrected into the r band using the transformation equation derived by Hillenbrand et al. (2018), in this case around 0.1 mag fainter. Data points from Herbst & Shevchenko (1999) are lower limits and based on their measured V -band brightness and an assumed $V - R > 3$ mag, then using the above conversion to r . Expansion of part of the ZTF time series appears in Figure 4.

source confusion issues arise when considering previously reported spectral types for LkH α 225.

In the early 1990s, LkH α 225 South clearly faded considerably, with the R -band magnitude increasing from the 14–15^m measured by Shevchenko et al. (1993) to the 17.3^m measured in 1993 by Hillenbrand et al. (1995). Based on early 1994 plate data, Magakian & Movsessian (1997) commented that the source was “virtually indiscernible even in I ”. Herbst & Shevchenko (1999) extended the Shevchenko et al. (1993) work to JD = 2450710 and documented continued fading to below $V = 24^m$, along with a color increase in the $V = 15$ – 19^m mag range from $V - R \approx 1$ to $V - R > 4.5$. An additional, previously unpublished faint-state measurement from 1999 is discussed below. Figure 2 shows that during this time period, LkH α 225 South was even fainter than LkH α 225 North.

By the time of the Sloan Digital Sky Survey (SDSS), in 2003, LkH α 225 South had brightened to once again become the brighter of the north–south pair, though no SDSS photometry is available at the source position.⁹ The INT/WFC Photometric H α Survey of the Northern Galactic Plane (iPhaS) measurements reported by Magakian et al. (2019) cover this missing SDSS epoch, however. The subsequent brightening of LkH α 225 South began some time between the last iPhaS epoch, in late 2006 (Barentsen et al. 2013), and the first Panoramic Survey Telescope & Rapid Response System (PanSTARRS) epoch in mid-2010 (Flewelling et al. 2020), as highlighted by Magakian et al. (2019).

Finally, a fortuitously timed set of observations taken by coauthor D.R.P. and reported to AAVSO (as user “RZD”), captured the photometric rise of LkH α 225 South during the period from 2014 August to 2015 September. This is between the PanSTARRS data acquisition and the mean epoch of the Gaia Data Release 2 (DR2) data point. Over the year, LkH α 225 South brightened by about 1 mag in R and reportedly also became somewhat redder in color, increasing from $V - R = 1.8$

to 2.2 mag. The first Magakian et al. (2019) observation is also in September 2015, and these authors measure a consistent $V - R = 2.08$ mag. Magakian et al. (2019) documented color variation at the ~ 0.1 – 0.2 mag level over the subsequent two years; see Figure 3.

3. Data Assembly Including Old Observations and New Data Acquisition

3.1. Imaging and Photometry

3.1.1. 1999 Keck Imaging Photometry

R_c - and I_c -band images of the entire BD+40° 4124 cluster including LkH α 225 South were taken in 1999 June using the Keck Low Resolution Imaging Spectrometer (LRIS; Oke et al. 1995). These data are illustrated in Figures 1 and 2 and have FWHM of $0''.54$ sampled at $0''.22$ pixel⁻¹. Astrometric calibration and photometry were performed soon thereafter, as follows. Within the IRAF environment, point sources were identified, centroided, and photometered using a 7 pixel aperture with a sky annulus extending from 10 to 20 pixels. This resulted in measurements for LkH α 225 North of $R_c = 19.40 \pm 0.01$ mag and $I_c = 17.60 \pm 0.01$ mag, and for LkH α 225 South of $R_c = 19.08 \pm 0.01$ mag and $I_c = 17.21 \pm 0.01$ mag. However, as can be seen in Figure 2, the faint state of LkH α 225 South reveals an even more complicated morphology with an additional, previously unappreciated, extension to the northeast.

The composite photometry from the 7 pixel aperture must therefore be decomposed. We recently reexamined these images to derive that the separation of the close pair is 3.78 LRIS pixels or $0''.83$ at PA = 35.5° from southeast to northwest. The LkH α 225 South-NE component is 0.35 mag brighter than LkH α 225 South itself. Adopting the combined NE+SW brightness as the 19.08 mag reported above, we find that the individual R_c -band brightnesses are 19.66 mag for LkH α 225 South-NE and 20.02 mag LkH α 225 South. As discussed in Section 4, it seems likely that this NE component is nebular rather than stellar.

⁹ There is a reported measurement at a position within the nebulosity between the northern and southern components. In fact, the north–south pair plus the connecting nebular ridge is categorized as a galaxy in SDSS catalogs (as also noticed by Magakian et al. 2019).

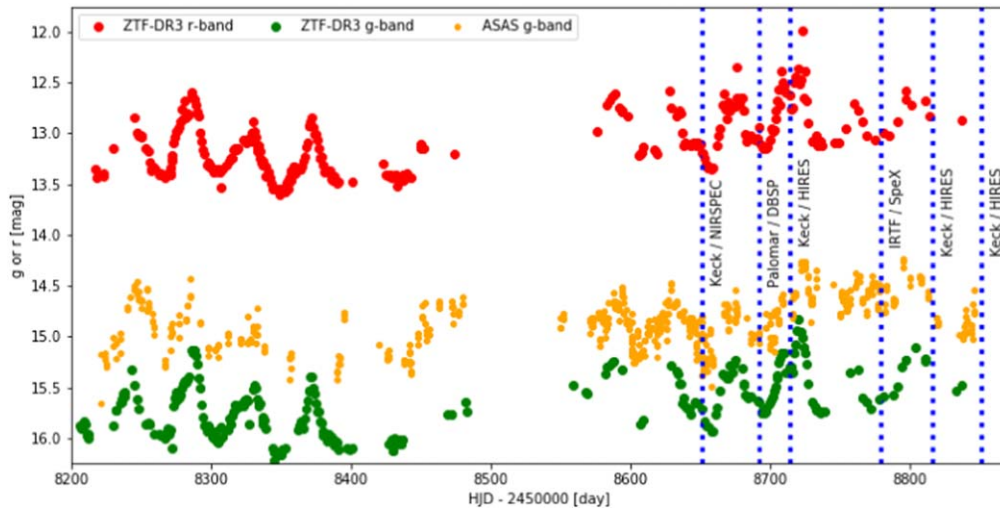


Figure 4. LkH α 225 South time series obtained in the r band and g band by the ZTF in the 2018 and 2019 seasons; error bars are plotted but are generally smaller than the points. The source is clearly quasiperiodic in the outburst state, with an oscillation timescale of a little more than a month. The g -band photometry reported by ASAS is also included. The ~ 1 mag offset between the ASAS and ZTF g -band measurements is likely a result of the large ASAS pixels; added variability from LkH α 225 North on top of the quasiperiodic variations exhibited by LkH α 225 South perhaps explains the inconsistencies, e.g., around MJD \approx 8350 and 8390 days. Epochs of spectroscopy are indicated and labeled.

3.1.2. 2018–2020 Optical Survey Photometry

The Zwicky Transient Facility (ZTF; Bellm et al. 2019; Graham et al. 2019) measured g and r photometry for LkH α 225 South over three seasons. Photometry was harvested from the IPAC/IRSA service¹⁰ (Masci et al. 2019), which provides >450 measurements in each filter. ZTF magnitudes are calibrated to PanSTARRS but do not have color corrections applied.

Over the same time period as the ZTF data set, the All Sky Automated Survey (ASAS; Shappee et al. 2014) was also observing the field in the g band. As illustrated in Figure 4, the ASAS light curve mimics the ZTF results, though the photometry is ~ 1 mag brighter. The offset between the ASAS and ZTF g -band measurements is not fully explainable by filter or photometric calibration differences, and likely resides in the large photometric aperture of ASAS, which would also encompass LkH α 225 North just $5''$ away.

3.1.3. Infrared Photometry Check

There is unfortunately no infrared monitoring photometry available for LkH α 225 South due to the brightness of the source itself and the crowding of bright sources in this complex region.

In the near-infrared, the J -band data stream coming from the Palomar-Gattini-IR survey (De et al. 2020) shows that the source of interest is both saturated and confused.

In the mid-infrared, we similarly come up short on recent monitoring data, though there is evidence that a brightening has occurred. LkH α 225 South is saturated in all four bands of the Wide-field Infrared Survey Explorer (WISE) data products and in the two bands of the NEOWISE reactivation mission. Furthermore, there is a slight positional offset to the west due to the nearby V1686 Cyg. However, earlier 2004 epoch measurements from Spitzer, as reported by Gutermuth et al. (2009), indicated $[3.6] = 5.6$ mag and $[4.5] = 4.4$ mag for LkH α 225 South and $[3.6] = 5.1$ mag and $[4.5] = 4.4$ mag for

V1686 Cyg. The existing WISE data (Cutri et al. 2012) from 2010 provide only lower limits on brightness due to saturation with $[3.4] < 3.3$ mag and $[4.6] < 1.8$ mag. Although there is contamination by the near-equal brightness V1686 Cyg, the WISE data indicate significant mid-infrared brightening of LkH α 225 South between 2004 and 2010. Furthermore, NEOWISE monitoring data (Cutri et al. 2015) between 2014 and 2018, which is also highly saturated, seem to indicate evidence for brightening from $[3.4] < 3.0$ to $[3.4] < 1.5$ mag. As all of the WISE/NEOWISE data are beyond the limits of any of the derived saturation corrections,¹¹ we are unable to comment further on the mid-infrared light curve of LkH α 225 South.

3.2. Spectroscopy

3.2.1. Optical

The venerable Double Spectrograph (Oke & Gunn 1982) was used at the Palomar 200'' telescope on 2019 July 27 (UT) to obtain flux-calibrated spectra of LkH α 225 South. The spectra cover ~ 3850 – 6800 Å with the 600/4000 grating on the blue side, at 1.08 Å/pixel sampling, and 7500 – 9000 Å with the 1200/7100 grating on the red side, at 0.40 Å pixel⁻¹. A $1''$ slit was used with the slit positioned at the parallactic angle. Spectra were extracted using the python package pyraf-dbsp,¹² developed by E. Bellm and B. Sesar, as a wrapper to IRAF data processing and spectral extraction tools. The realized S/N ranges from ~ 10 in the far blue to ~ 100 in the far red. The resulting optical spectra are illustrated in Figures 5 and 6.

We obtained an optical echelle spectrum between ~ 3400 – 7900 Å at resolution $R \approx 60,000$ using the Keck I telescope and HIRES (Vogt et al. 1994) on 2019 August 18 (UT). Data acquisition used the standard operating procedures of the California Planet Search as described in Howard et al. (2010).

¹⁰ <https://irsa.ipac.caltech.edu/cgi-bin/Gator/nph-scan?submit=Select&projshort=ZTF>

¹¹ http://wise2.ipac.caltech.edu/docs/release/neowise/expsup/sec2_1civa.html

¹² <https://github.com/ebellm/pyraf-dbsp>

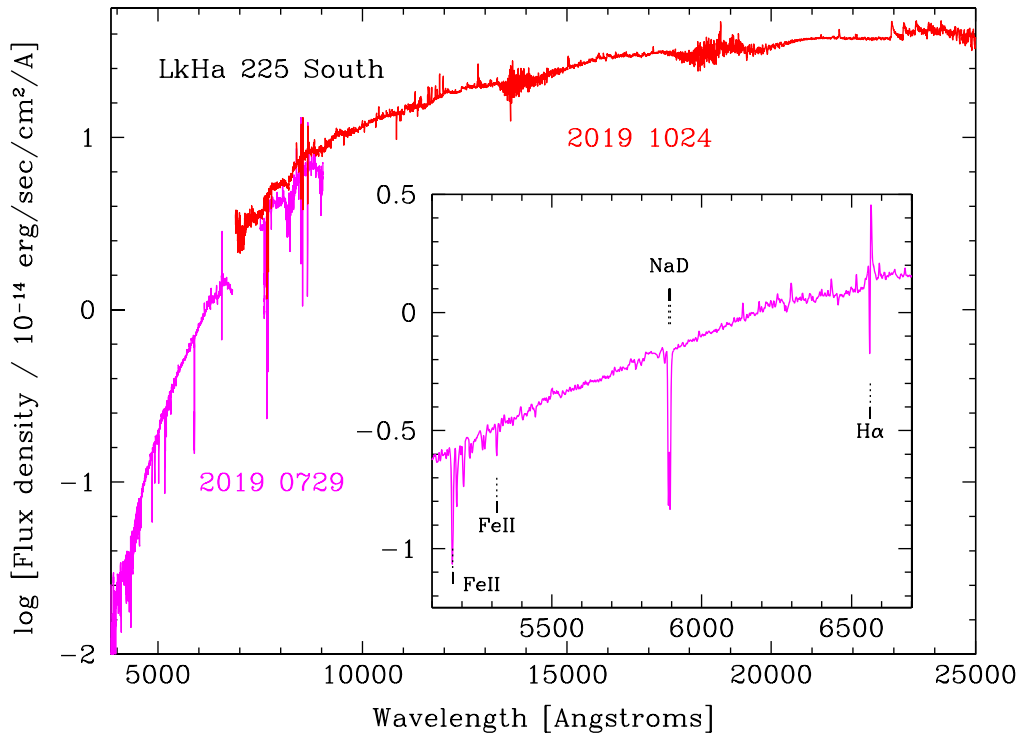


Figure 5. LkH α 225 South low-dispersion optical spectrum from Palomar/DBSP (magenta) and infrared spectrum from IRTF/SpEx (red). LkH α 225 South appears significantly reddened, even in outburst. Figures 6 and 9, respectively, offer expanded views of the optical and infrared portions of the spectra. Inset illustrates the strong Na iD and H α features; both have blueshifted absorption components when examined in higher spectral dispersion data (see Figure 11).

A 635 s exposure resulted in a spectrum with $S/N = 45$ at 5600 \AA and $S/N \approx 150$ at 7100 \AA .

Two additional HIRES spectra were obtained on 2019 November 29 (UT) and 2020 January 3 (UT), both covering $\sim 4800\text{--}9200 \text{\AA}$ at resolution $R \approx 25,000$. These were processed using the MAKEE reduction pipeline¹³ written by T. Barlow.

3.2.2. Infrared

We obtained spectra in the 1 μm Y -band region at $R \approx 18,500$ with the Keck II telescope and the recently upgraded (Martin et al. 2018) NIRSPEC (McLean et al. 1998) instrument. The $0''.576$ slit was used with rounds of A-B-B-A position nods taken with exposure times of 30 s per position. Spectra were taken on 2019 June 16 (UT) by E. Petigura and T. David, and on 2020 September 2 (UT) by L.A. H. and J. Spake. The data were processed using the REDSPEC package written by L. Prato, S.S. Kim, and I.S. McLean.

We also observed LkH α 225 South over a broader spectral range, covering 0.7–2.4 μm at a resolution $R \approx 2000$ with the IRTF and SpeX (Rayner et al. 2003) in its short-wavelength cross-dispersed (SXD) mode. On 2019 October 24 (UT) a set of 15 s exposures were taken with 4 minutes of total exposure time through the $0''.3$ slit. The realized S/N per exposure is ~ 60 in the Y band and ~ 200 in the K band.

Finally, we make use of IRTF/SpEx spectra of LkH α 225 South obtained in a much earlier stage of the long-term outburst, closer to the faint state, in fact. On 2003 May 31 (UT) the $0''.5$ slit was used to obtain SXD and long-wavelength cross-dispersed (LXD) data covering 1–4 μm for both LkH α 225 South and LkH α 225 North. These spectra are illustrated in

Figure 7. Below we compare this older LkH α 225 South spectrum to the more recent spectrum taken in the outburst state.

4. Small-scale Morphology of the LkH α 225 Environment

The complexity of the region under study was increased by the revelation provided in our 1999 Keck/LRIS images that, in its faint state, LkH α 225 consists not only of the well-known wide separation ($5''$) north–south pair, but an additional spatially resolved component on smaller scales. This newly appreciated source has a separation of $0''.8$ from LkH α 225 South (Figure 2).

Careful consideration of the astrometry shows that the source currently outbursting and identified as LkH α 225 South, specifically as measured by Gaia Collaboration et al. (2018), coincides with the fainter southwest optical component of the close pair in Figure 2. The northeast component was brighter in 1999, with an east–west extension that indicates it may be nebular.

The next available imaging data at sufficiently high spatial resolution is a 2003 infrared image from the Gemini Science Archive, shown in Figure 7. The southwest component is clearly seen as the much brighter source at this epoch, while the northeast component is still apparent. The H $_2$ emission aspect of the northeast component can be isolated by subtracting a spatially registered and scaled continuum image. We do not show such a subtracted image due to strong residuals induced by a temporally variable adaptive optics point-spread function, which affects the image alignment and subtraction results. However, we can report that such a subtraction retains only the extended structure several arcsecs to the northeast and several arcsecs to the west-southwest of LkH α 225 South, as well as the very diffuse material to the northeast of V1686 Cyg.

¹³ <https://astro.caltech.edu/~tb/makee/>

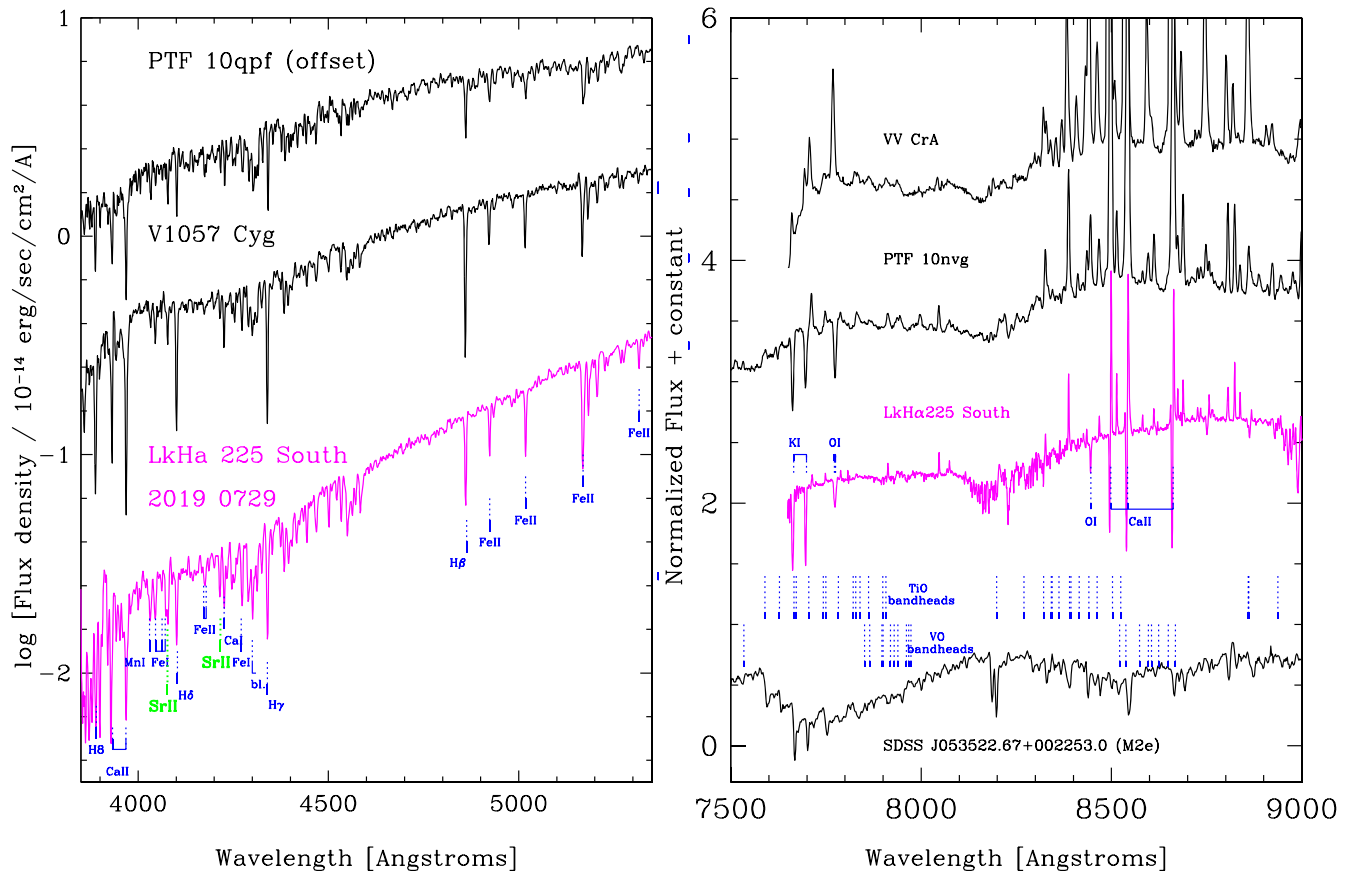


Figure 6. Portions of the Palomar/DBSP optical spectrum of LkH α 225 South (magenta) compared to other young stellar objects with rare spectral signatures. Left panel highlights absorption in LkH α 225 South throughout the blue spectral range, with comparison made to the FU Ori stars V1057 Cyg and V2493 Cyg (PTF 10qpf; HBC 722). Right panel highlights the prominent TiO emission in the red, with comparison made to the bright states of PTF 10nvg (Covey et al. 2011) and VV CrA (Herczeg & Hillenbrand 2014); an example field M dwarf with TiO in absorption is also shown.

The compact nebular component that we are labeling as northeast of the point source LkH α 225 South seems coincident with the location of the maser spot field reported by Marvel (2005), as indicated in their Figure 7. This is likely also the same position as the 3.1 mm continuum peak reported by Looney et al. (2006). These coincidences suggest the possibility of an even more deeply embedded companion in the LkH α 225 system. Specifically, the optical and infrared nebulosity we see near this same position could be scattered light (H α and H $_2$ emission) that escapes along an outflow cone from a protostellar source.

The physical (projected) source separation between the southwest and nebular northeast sources can be calculated using Gaia DR2 (Gaia Collaboration et al. 2018) parallaxes. The reported parallax of LkH α 225 South itself is rather uncertain, and a high renormalized unit weight error is reported with RUWE = 8.1, whereas <1.4 is recommended. The nearby source V1686 Cyg also has a large parallax error. We thus use the parallax of the optically brightest source in the vicinity, BD +40 $^\circ$ 4124 (1.092 ± 0.031 mas), which is better determined. Adopting 916 pc as the distance to the region, the projected separation of northeast-southeast is 760 au, while the southwest (LkH α 225 South) to LkH α 225 North projected separation is about 4575 au.

Regardless of the nature of this northeast component, we do confirm after considerable astrometric analysis that the currently outbursting source is the well-known LkH α 225 South.

5. Photometric and Spectrophotometric Analysis

In its current outburst state, LkH α 225 South is red throughout the optical and near-infrared wavelength range, as illustrated in Figure 5. The overall red continuum slope has a number of contributors, including a central stellar source, gas and dust emission likely over a range of temperatures, and dust extinction from both the circumstellar and the local cloud environment.

5.1. Faint State to Bright State Changes

While LkH α 225 South remains red in an absolute sense, the optical colors in the outburst state seem somewhat, though not dramatically, bluer than those measured much earlier. The $g-r$ color of 2.8 mag (AB) reported by the ZTF would correspond to $V-R \approx 1.9$ mag and $R-I \approx 1.5$ mag. This is based on a conversion from $g-r$ (AB) to $V-R$ (AB) from Jordi et al. (2006), further correction from AB to Vega magnitudes, and then scaling $V-R$ to $R-I$ according to the relation between these colors in the LkH α 225 South monitoring data of Shevchenko et al. (1993).

The source colors were similar in the periods in the 1980s, before the long-duration fade to $>20^m$, as well as during the fade, e.g., the 1994 data (Hillenbrand et al. 1995; $V-R_c = 1.8$: mag and $R_c - I_c = 1.7$: mag), and within the deep fade, e.g., the 1999 Keck/LRIS imaging (Section 3.1; $R_c - I_c = 1.87$ mag).

Color information during the rebrightening is scarce. The 2014 measurements by coauthor D.R.P. that were reported to

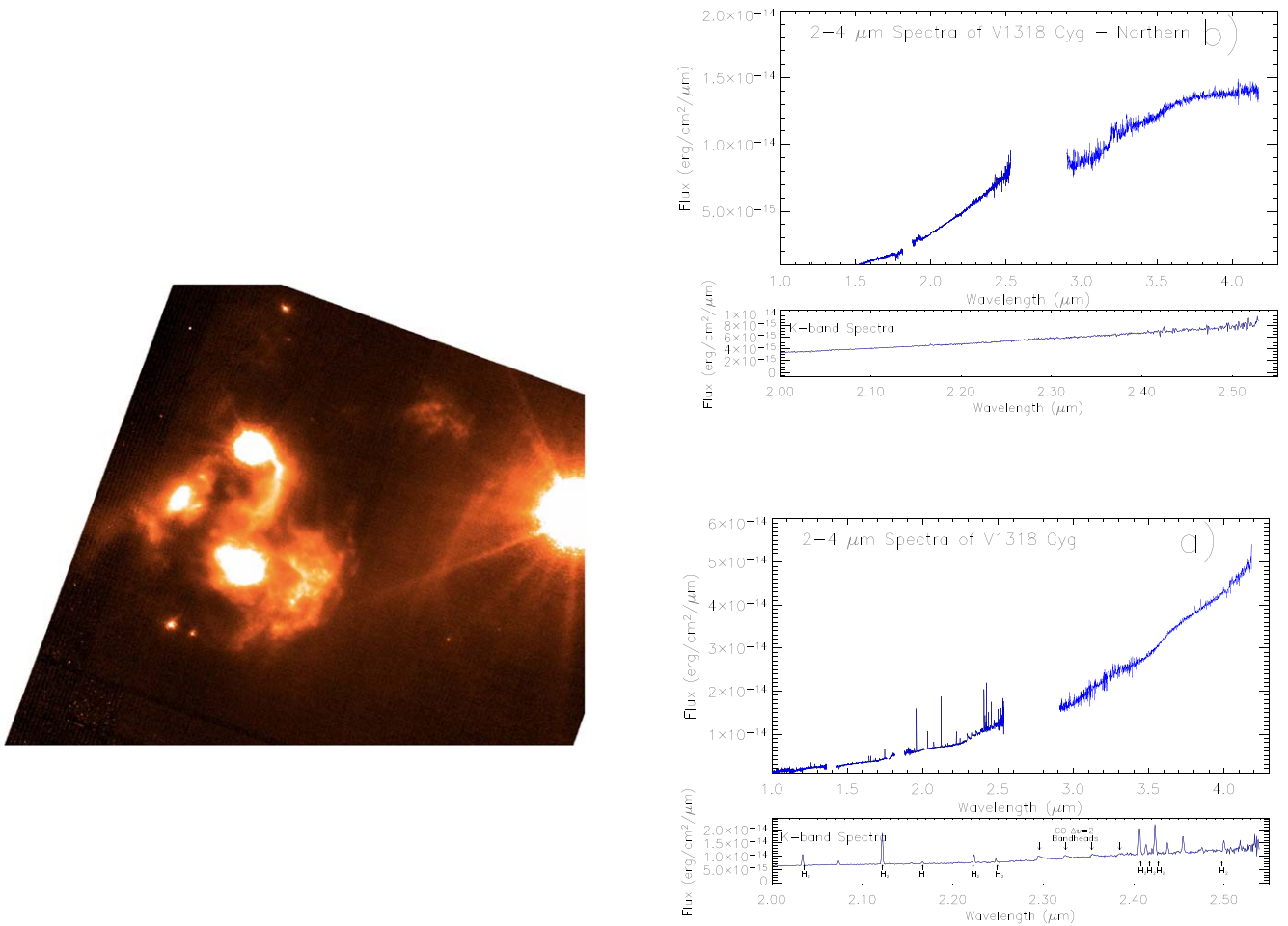


Figure 7. Left panel: 2003 Gemini/Near-Infrared Imager image in H_2 2.12 μm . The ridge of nebulosity extending southward from LkH α 225 North, which is apparent in optical images, is present in the near-infrared, as well. Also familiar is the compact nebulosity just northeast of LkH α 225 South, which was seen in our 1999 optical image (Figure 2). Several additional extended nebulosities appear in H_2 that are not seen in the optical. Right panels: spectra taken in 2003 of LkH α 225 North (labeled V1318 Cyg North) and LkH α 225 South (labeled V1318 Cyg South), during the faint state of the latter. The 1–4 μm data show a red continuum in both components of LkH α 225. Lower plots in each case highlight the K -band spectral region.

AAVSO (as user “RZD”) were $V - R = 1.7 - 2.2$ mag. They show the $V - R$ color becoming redder as the source brightens by about 0.6 mag. This is consistent with the fact that the currently measured $g - r = 2.8$ mag (AB) is redder than the PanSTARRS values of $g - r = 2.1$ mag (AB), measured in 2013, and 2.3 mag (AB), measured in 2011. The current values are on the blue side of the colors measured in 2015 by Magakian et al. (2019), which also represent the bright state, reported as $V - R = 2.1$ mag and $R - I = 1.5 - 1.8$ mag.

We note that for the majority of these photometric measurements, the errors are often unreported. As a guide to approximate values, we consider that the $g - r$ color error in the PanSTARRS (PS1) catalog is 0.1 mag, and we take this as a minimum error for the other color measurements given above.

Even though the current optical colors do not seem significantly different from those measured at much earlier epochs, the evidence seems to suggest a reddening trend as the source rose to its current peak brightness. However, this is not what is seen in the infrared.

Although no colors are available, we do have spectrophotometric measurements. To determine whether the infrared SED has changed during the brightening, we can directly examine the 2003 infrared spectrum relative to the 2019 infrared spectrum; both are illustrated in Figure 9. A ratio of the

two spectra shows a flux increase during the burst by a factor of ~ 100 in the J band, ~ 85 in the H band, and ~ 50 in the K band, implying a “blue” nature to the burst.

5.2. Extinction Effects

There is no value of extinction that would truly flatten the infrared flux ratio spectrum described above. This implies that the dramatic brightening can not be explained by a reduction in extinction alone. However, a decrease in A_V by about 3 mag would nearly equate the ratio at the J band and K band around a value of ~ 35 , with the H band a little higher. A reasonable scenario is one in which there has been both a reduction in line-of-sight extinction to the infrared continuum, and intrinsic source brightening.

The total line-of-sight extinction is harder to evaluate. A recent estimate by Carvalho & Hillenbrand (2022) makes use of diffuse interstellar bands (DIBs) absorption features to estimate $A_V = 2.7$ mag for $R_V = 3.1$ and $A_V = 4.3$ for $R_V = 5$. This is absorption against the outburst optical continuum. Here, we find that dereddening the flux-calibrated optical outburst spectrum by A_V values in the range 4–9 mag produces an SED at blue wavelengths that is consistent with unreddened FGK stellar templates (with the higher A_V values corresponding to the earlier templates). Again, these estimates would be the

current extinction to the source of the optical continuum. An additional $A_V \approx 3$ mag is needed to describe the difference between the bright-state and faint-state infrared spectral slopes, meaning that the faint-state extinction was in the range $A_V = 6\text{--}12$ mag.

This range of A_V values is consistent with what can be inferred from the [Fe II] lines in the faint-state (2003) infrared spectrum. We use the formalism of Pecchioli et al. (2016) with the intrinsic line ratios of Bautista et al. (2015) and reddening law of Fitzpatrick (1999). From the measured [Fe II] 1.257, 1.321, and 1.644 μm line fluxes of 1.47, 0.47, and 2.13×10^{-14} , respectively, we find values $A_V = 7.3 \pm 0.1$ for $R_V = 3.1$. We can not derive a value for the bright-state (2019) spectrum since the continuum brightening renders the [Fe II] lines immeasurable.

It is unclear how much of the total line-of-sight extinction should be attributed to the molecular cloud and how much to the circumstellar environment, but we note that the long-wavelength portion of the pre-outburst spectrum (Figure 7) does not show evidence of the 3 μm water ice feature, which is often associated with high-extinction, high-density environments. The lower among the above extinction values may thus be most appropriate.

5.3. Bright-state Quasiperiodicity

To assess the periodicity of the photometric oscillations seen in Figure 4, we employed a Lomb–Scargle period search algorithm (see, e.g., VanderPlas 2018, for a thorough discussion) as implemented in the LombScargleFast routine under the gatspy.periodic python package. The period was fit in flux units rather than in magnitudes. Using the full ZTF data set, a single strong peak in the periodogram corresponds to a derived period of 43.4 days. While the period has persisted for three years, there is some evidence for a fluctuation over time in the mean source brightness, on top of which the periodicity resides. Including a fit for this drift does not change the mean period or amplitude, but does reduce the scatter as a function of phase. The mean r -band magnitude was 13.0 mag during the 2018 season, which brightened to $r = 12.6$ mag during the 2019 season, then faded to $r = 13.3$ mag during the 2020 season. In addition, within the seasons, we find that in 2018 there was a downward drift corresponding to 0.42 mag yr^{-1} , in 2019 an upward drift of $-0.32 \text{ mag yr}^{-1}$, and in 2020 the source was fading by 0.22 mag yr^{-1} . Correcting for these drifts and phasing the light curve results in the profile shown in Figure 8.

Among individual cycles, the amplitude of the periodic signal ranges from ~ 0.6 to ~ 0.8 mag. A formal analysis using a smoothed version of the light curves yields peak-to-trough amplitudes of 0.66 ± 0.05 mag for the r band and 0.68 ± 0.14 mag for the g band. The light-curve peak-to-trough excursion time is nearly one-half of the period, with the derived time between light-curve maximum and light-curve minimum 0.48 ± 0.10 times the period for both r band and g band. Notably, the clear periodicity in the g and r light curves comes without any change in color. We find an essentially constant value over time $g - r = 2.8$ mag (AB) and no evidence for color periodicity in the source.¹⁴

¹⁴ The only color periodicity appears to be a few percent signal associated with the ~ 28 day cycle of the moon phase. This period is also seen as a low-level brightness periodicity, though at a factor of ten lower significance than the ~ 43 day astrophysical peak.

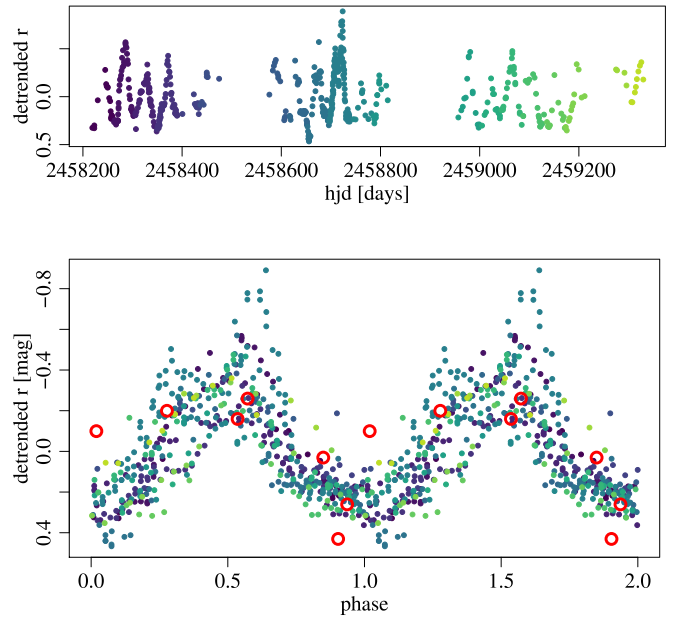


Figure 8. Top: ZTF r -band light curve with linear detrending performed separately for the 2018, 2019, and 2020 seasons. Color scale shows a progression of hues from earlier to later cycles. Bottom: phased light curve for a period of 43.4 days, repeated twice so as to more readily discern the full-phase shape. Larger red points are the seven data points from Magakian et al. (2019).

We note that the current periodicity can not be recovered in available photometry from earlier epochs (Figure 3). Specifically, neither the 2015–2017 data of Magakian et al. (2019) nor the 1980s data of Shevchenko et al. (1993) show detectable periodicity. However, we have checked whether the Magakian et al. (2019) data can be phased to the currently observed period. As shown in Figure 8, the fluctuations seem significant and tend to display the same trends as the current data, but phase up with two of the seven points having more scatter than the recent ZTF data.

6. Spectroscopic Analysis

The subsections below present the salient details of the LkH α 225 South spectral features. We begin by comparing the outburst infrared spectrum to an earlier pre-outburst spectrum, highlighting changes. We then proceed to discuss the various spectral elements of the outburst spectrum in detail. There is evidence of a strong wind/outflow seen against the optical continuum, but not of a shocked atomic gas component, which would manifest as, e.g., strong forbidden lines formed in a jet. However, there are weak shocked gas emission signatures in molecular H_2 and atomic [Fe II] in the infrared that have weakened relative to the continuum during the outburst. The outburst also features molecular TiO and CO emission and weak atomic metal line emission that appears mainly at wavelengths longer than ~ 6000 \AA . Finally, there is photospheric absorption that apparently arises from a low-gravity atmosphere having mixed temperature, with both hot features (e.g., Fe II) at blue wavelengths and cool features (e.g., H_2O) at red wavelengths. After the following detailed description of the outburst spectrum, we close the section by describing the subtle differences among the three HIRES spectra taken at moderately different photometric phases.

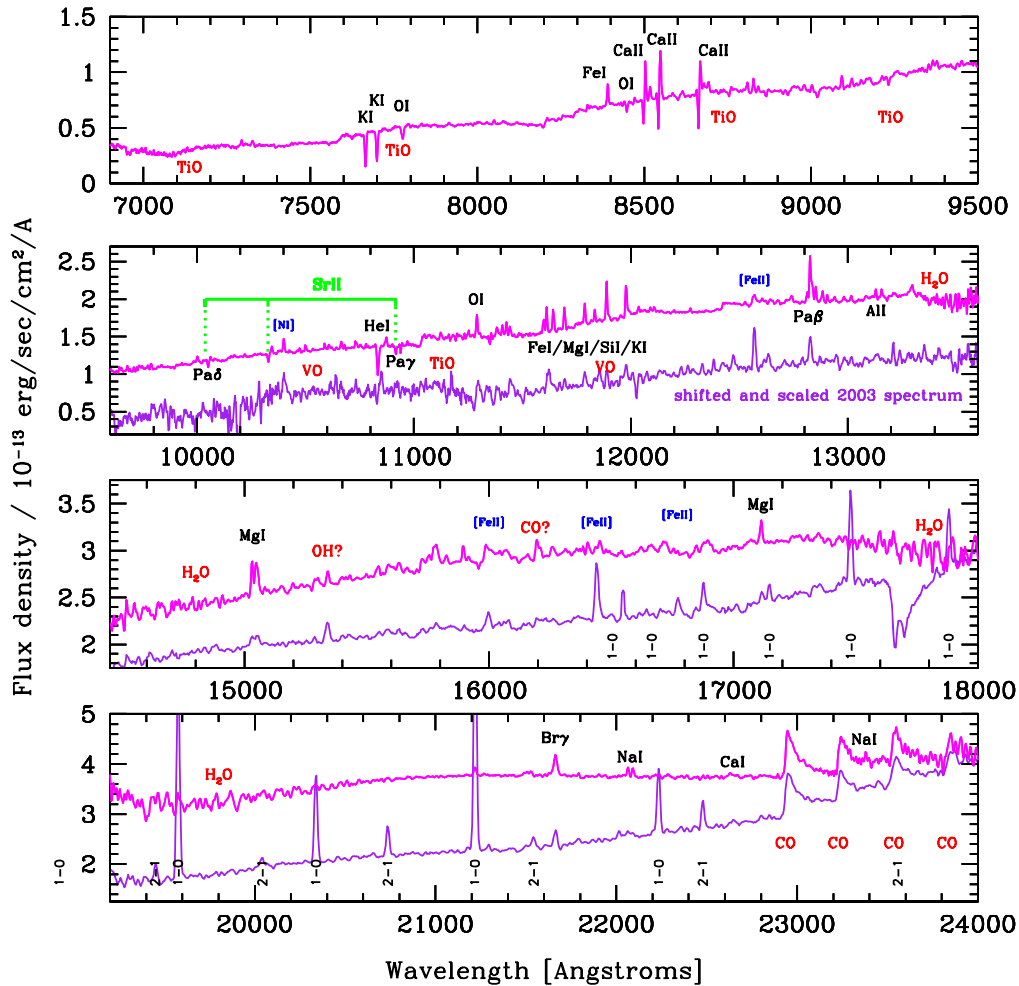


Figure 9. IRTF/SpEx data comparing the 2019 outburst spectrum (upper, magenta) with a version of the 2003 faint-state spectrum (lower, purple) that has been scaled (by a factor of 50) and shifted (individually in each panel). In the faint state, LkH α 225 South exhibited relatively weak atomic emission features but strong molecular emission from H $_2$ (labeled as 2-1 or 1-0) and CO bands. During the brightening from 2003 to 2019, the LkH α 225 South infrared continuum has become bluer though it is still extremely red on an absolute scale. The line-to-continuum ratio of the weak atomic emission has increased, while the line-to-continuum of the previously prominent H $_2$ lines has become weaker; the CO line-to-continuum appears relatively unchanged.

6.1. Spectral Changes between 2003 and 2019

The spectral ratio analysis described above reveals that the H $_2$ O absorption seen in Figures 9 and 10 has been enhanced during the outburst. Another finding is that there is essentially no change in the CO line-to-continuum, with only continuum remaining in this wavelength region of the ratio spectrum. Any change in TiO is hard to assess, as it is not possible to determine whether or not the source had TiO before the long-duration outburst. Also, the prominence of narrow H $_2$ emission relative to the continuum has decreased in the bright state.

Regarding the atomic emission, detailed examination shows that essentially all of the 1–2.4 μ m lines now seen in emission in the bright state were also present in the faint state. The atomic emission-line pattern is essentially the same, only weaker in the earlier spectrum. The ratio spectrum shows no change in the line-to-continuum, i.e., no signature of the emission lines in the ratio spectrum. The implication is that the photometric brightening contributes equally to the continuum and the atomic line emission.

Going back even further, the near-infrared spectra shown in Aspin et al. (1994), taken in 1991, compare very well to those illustrated in Figure 7, taken in 2003. The earlier date closely follows the end of the Shevchenko et al. (1993) time-series data

illustrated in Figure 3, which is just before the deep fade¹⁵ from $\sim 15^m$ to $\sim 19^m$. The 2003 date was firmly in the deep fade. Thus, the fading and accompanying reddening (Herbst & Shevchenko 1999) do not seem to have resulted in any change in the source spectrum. Conversely, the brightening from $\sim 19^m$ to the current $\sim 13^m$ has produced a change in the emission and absorption spectrum in the K band (Figure 10).

6.2. Wind and Jet Outflow Lines

Seen against the very red continuum are a number of indicators of rapidly outflowing gas from LkH α 225 South. Figure 11 illustrates deep, blueshifted absorption in the usual prominent optical wind lines, notably Mg Ib, Na ID, K I 7665 and 7699 Å, and O I triplet. Wind signature is even seen in Li I 6708 Å. H α , along with the Ca II triplet lines (Figure 12), exhibit P Cygni structure.

The Na ID wind absorption is saturated, and the K I nearly so. We note explicitly that the wind evidenced in the red lines of K I, O I, and Ca II is forming against the continuum of the molecular TiO/VO emission. At bluer wavelengths, absorption

¹⁵ Aspin et al. (1994) report fading by 2 mag in the near-infrared between 1991 October and 1993 November.

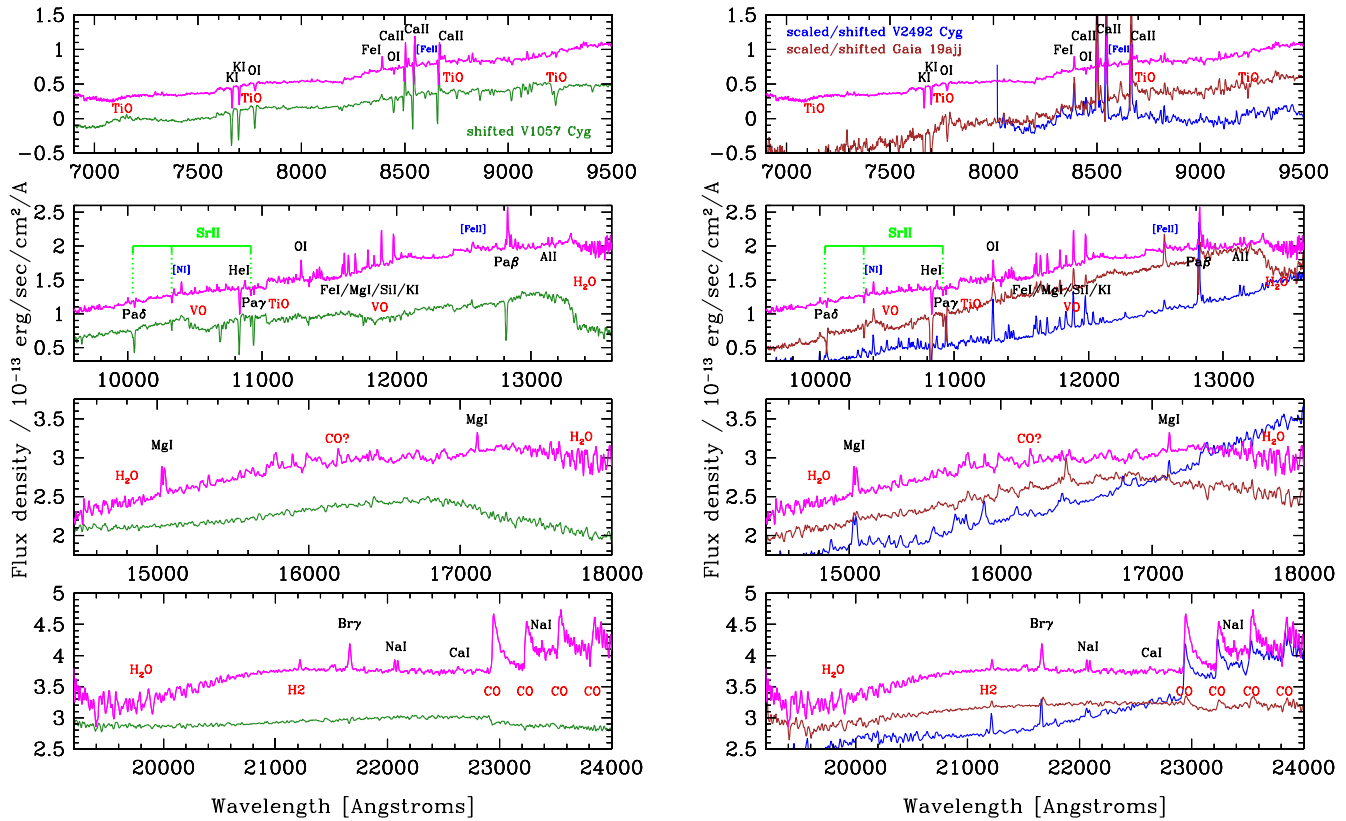


Figure 10. Left panels: comparison of LkH α 225 South (magenta) and V1057 Cyg (green) at infrared wavelengths. These sources are a reasonable match in terms of their absorption features at blue optical wavelengths in low- (Figure 6) and high- (Figure 14) spectral-resolution data. This is also true at red optical wavelengths (top panel), including the TiO emission shared by both sources. At >9000 Å, however, the spectral match is less good, with LkH α 225 South lacking the strong molecular H $_2$ O, as well as the TiO, VO, and CO absorption that is seen in V1057 Cyg at these longer wavelengths. The redward side of the *J* band and the *H* band does indicate some weak H $_2$ O, however. In addition, rather than CO absorption, LkH α 225 South has strong CO emission, as well as other atomic emission lines that are more reminiscent of other types of young-star outbursting sources. Right panels: the same LkH α 225 South spectrum as in the left panels (magenta) now compared to V2492 Cyg (blue) and Gaia 19ajj (brown). LkH α 225 South shares the weak H $_2$ O absorption in the *J* band and *H* band with Gaia 19ajj, though the TiO and VO patterns differ slightly. The CO emission of LkH α 225 South is more similar to V2492 Cyg than Gaia 19ajj, and the atomic emission-line patterns better match this source, as well. The only atomic absorption in LkH α 225 South is from Sr II (see also Figure 13), which is also seen in both V1057 Cyg and Gaia 19ajj.

in lines of Fe II, such as 4172, 4179, 4924, 5018, 5169, 5197, 5234, and 5316 Å, is evident in our low-resolution spectra (e.g., Figure 6) and revealed in our higher resolution spectra (not shown) to also have broad blue asymmetry, indicative of a wind. The typical terminal velocity of these metal lines is about -150 km s $^{-1}$.

The H α and Ca II triplet lines are strong and broad. However, the entire blueshifted portion of the emission profile is not, in fact, absorbed. Instead, the absorption extends to about -210 km s $^{-1}$ with an additional wing of unabsorbed blueshifted emission that extends to about -325 km s $^{-1}$ (see Figures 11 and 12). At low dispersion, our H α profile appears very similar to the time series of such profiles that are shown in Figure 4 of Magakian et al. (2019).

In the infrared, Figure 10 indicates Br γ and Pa β strongly in emission, but the resolution is too low to discern the line kinematics. The Pa γ line is ambiguously present in Figure 10, but Figure 13 shows this line at higher dispersion. It has a clear P Cygni profile, indicating wind signature in our 2019 spectrum, but the 2020 spectrum shows the line in pure absorption, centered at zero velocity.

Figure 13 also shows the He I 10830 Å triplet profile, which has a depth of about 70% of the continuum and width ± 200 km s $^{-1}$. The profile is fairly symmetric around the weighted line center of the triplet. Furthermore, the absorption is broader than that exhibited in the nearby hydrogen or metal lines. There is

no obvious P Cygni structure or blueshifted asymmetry in He I 10830. In other young-star outbursters He I 10830 line depths can reach to only $\sim 5\%$ of the continuum in some cases. One object with a He I 10830 profile that is quite similar to that of LkH α 225 South is FU Ori itself, with similar centroid, width, and depth.

Notably, there is no change in the He I 10830 Å profile between our two spectra taken approximately 1.2 yr apart. As stated in the Introduction (Section 1), an early spectrum of Andrillat & Swings (1976) also showed strong absorption in the He I 10830 Å line. There is indication of such in the 2003 IRTF/SpeX spectrum, as well (see Figure 9), possibly with a P Cygni-type profile, which is not present in the current outburst state.

Regarding forbidden line emission, we do not see a strong signature in the [O I] or [S II] lines that are reported as detected by Magakian et al. (2019). However, these authors acknowledge that bad sky subtraction could be an issue in their data, and could cause a false positive. The source is not significantly different in brightness now compared to the Magakian et al. (2019) observations, so continuum brightening is not the explanation for the lack of detection of these lines in our data. We do find, however, unambiguous [Ca II] doublet emission at 7291 and 7324 Å (Figure 12). This doublet is rarely seen in normally accreting young sources, though it was seen in the outbursting case of PTF 14jg (Hillenbrand et al. 2019a). The

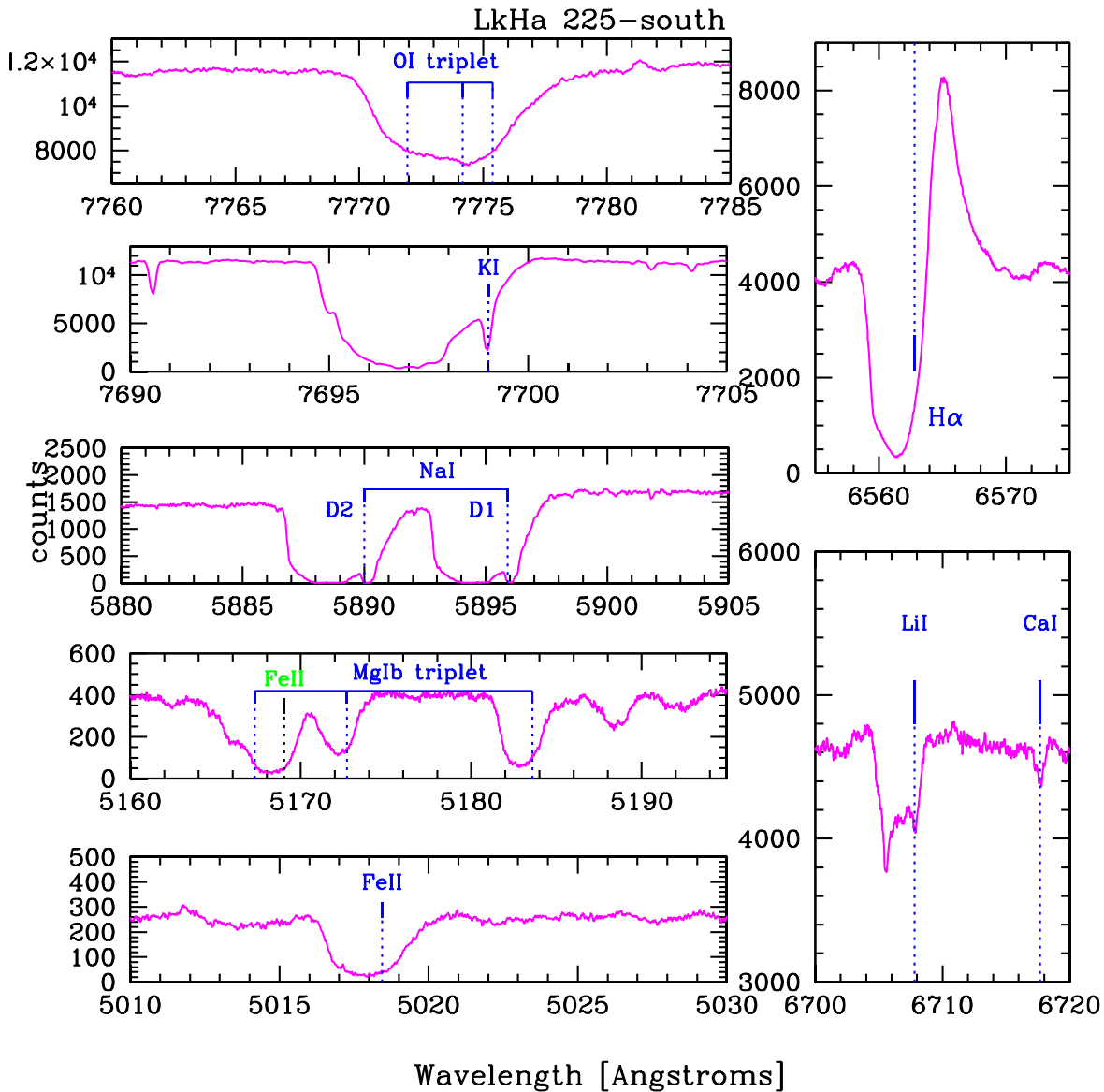


Figure 11. Portions of the 2019 August Keck/HIRES spectrum illustrating the strong wind of LkH α 225 South via blueshifted absorption features. In the lower-right panel, the narrower Ca I absorption line validates the wavelength scale and thus our heliocentric correction to the stellar rest velocity. The H α profile (upper-right panel) has a clear P Cygni nature, with the absorption against the emission profile extending to about -210 km s^{-1} on the blue side, though the emission wing continues to about -325 km s^{-1} . The red-side emission peaks at $+85 \text{ km s}^{-1}$ and extends to $+275 \text{ km s}^{-1}$. Broad blueshifted absorption is also seen in Li I (lower-right panel), and the K I doublet, the O I triplet, the Na I D doublet lines, the Mg I b triplet lines, and among the wind-sensitive Fe II lines. The typical terminal velocity in the metal lines is -150 km s^{-1} .

[Ca II] doublet is the only strongly detected optical forbidden line in the outburst state of LkH α 225 South.

6.3. Molecular Emission

Molecular emission in the form of H $_2$ is associated with shocked gas in near-circumstellar environments. This molecule is only weakly seen in the K-band region of LkH α 225 South in its outburst state. Comparing the recent outburst spectrum to the earlier 2003 pre-outburst or early outburst spectrum, the H $_2$ line-to-continuum is weaker in the outburst spectrum, as discussed above.

More unusual, in terms of molecular features, is that in outburst LkH α 225 South exhibits the rare phenomenon of having TiO bands in emission. This is seen from the red optical out to the 11300 Å band (Figures 6 and 10). There is a hint that the 11300 Å emission was also present in the pre-outburst state

(Figure 9). Only a few young stars have been documented with TiO in emission, specifically PTF 10nvg/V2492 Cyg (Covey et al. 2011), IRAS 04369+2539 and IRAS 05451+0037 (Hillenbrand et al. 2012), VV CrA (Herczeg & Hillenbrand 2014), iPTF15afq (Miller et al. 2015, a.k.a. Gaia19fct), and PGIRN 20dwf (Hankins et al. 2020, a.k.a. Gaia20eae). Figure 10 demonstrates V1057 Cyg to be in this category, as well: the spectrum is the same as that shown in Connelley & Reipurth (2018), though the TiO emission aspect was not commented upon in that paper.

Typically, TiO and VO bands are seen in absorption, and signify the presence of warm molecular gas ($\sim 1500\text{--}4000 \text{ K}$) in a cool stellar atmosphere. These molecules define the onset of the M-type spectral class, for example, with increasing absorption seen in the TiO/VO species toward later types, transitioning to CO and H $_2$ O molecules at even cooler M-type

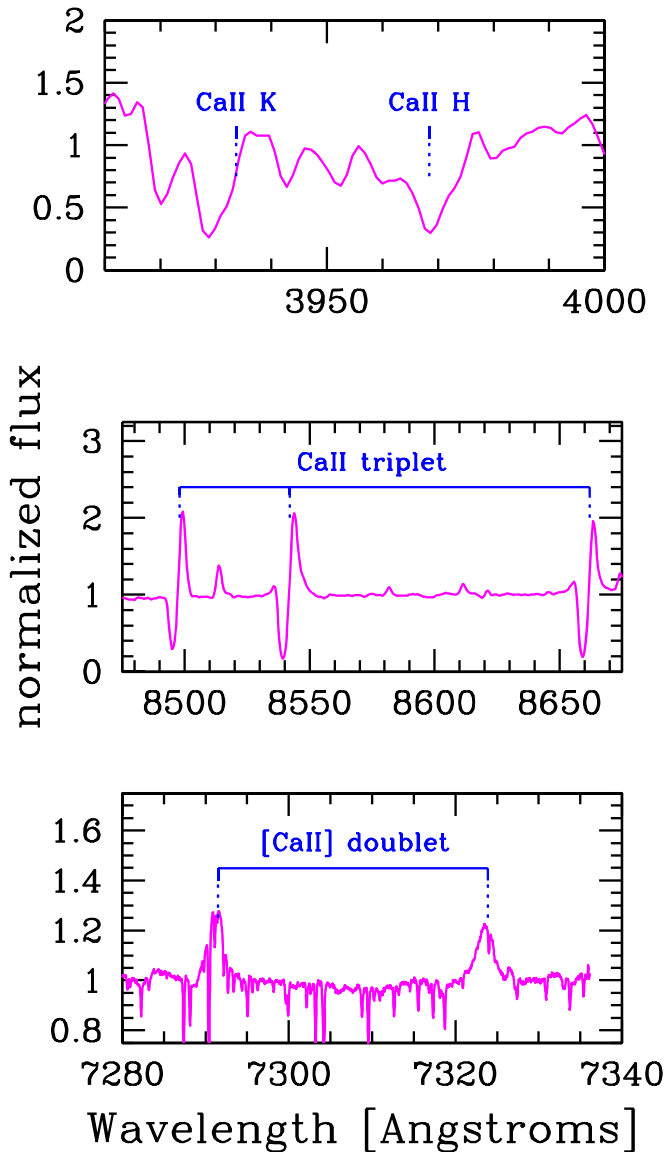


Figure 12. The optical ionized calcium lines in LkH α 225 South. Top and middle panels show the permitted transitions of Ca II as seen in the Palomar/DBSP spectrum, while the bottom panel shows the forbidden transitions of [Ca II] as seen in the Keck/HIRES spectra (with uncorrected telluric absorption contamination still present in the data).

photospheres. All four of these molecules are observed in absorption from the disk atmospheres associated with FU Ori stars (Connelley & Reipurth 2018).

In LkH α 225 South, we see the optical and near-infrared TiO/VO bands, and the infrared CO lines, all in emission, but the H₂O molecule is in absorption.

6.4. Atomic Emission

There is sparse, weak, narrow atomic emission in the outburst spectrum of LkH α 225 South. The lines are at the rest velocity, and overall the narrow emission spectrum is quite similar to that of V2492 Cyg, suggesting a similar temperature, though weaker in terms of line strength.

In the optical, the emission is seen mainly at the redder wavelengths of Figure 6, with little emission detected shortward of ~ 6000 Å, even at high spectral resolution. The optical lines are mainly Fe I with some Ni I and Ti I. There is an

apparent trend in emission versus absorption with line excitation energy. Many lower-excitation Fe I and Ni I lines are weakly in emission, but the higher-excitation lines in these same neutral species are seen mainly in absorption.

At infrared wavelengths, as depicted in Figure 9, there is a slightly stronger, well-populated atomic emission-line forest in the *J* band. There is also weak Mg I in the *H* band, and weak Na I and Ca I in the *K* band.

Magakian et al. (2019) reported that many (optical) lines of Fe II are in emission, which we do not see. Our spectra were taken approximately 4 yr later and show these same Fe II lines ubiquitously and unambiguously in absorption. This suggests cooling spectral evolution after the source reached its peak brightness. However, the low-excitation Fe I lines remain in emission. The situation in LkH α 225 South seems somewhat similar to the one in PTF 14jg, which was categorized by Hillenbrand et al. (2019a) as an unusually hot accretion outburst. That source exhibited strong absorption in Fe II, as well as in other even hotter ionized metals, early on in its outburst. PTF 14jg also showed Fe I and other neutral metal emission lines at the same early times, but these lines faded over several years and became absorption features.

6.5. The Pure Absorption Spectrum

The LkH α 225 South absorption spectrum is peculiar, and not readily interpreted as either a normal single star or a binary-star system. Instead, we suggest a more complicated composite spectrum.

Atomic absorption lines become increasingly prominent toward shorter wavelengths—down to the <4000 Å limit of our data. The photosphere of LkH α 225 South is thus apparently not heavily veiled in the blue. Veiling, or accretion continuum emission that occupies a low filling factor, would weaken the absorption lines. It arises under situations where the accretion rate is modest.

For higher accretion rates, it is possible to produce a predominantly absorbing spectrum that originates in the hot inner regions of an accretion disk. In this scenario, the bluer wavelength absorption lines we observe could originate in such a disk or a wind emanating from this same region. A relatively cooler emission-line component would fill in the low-excitation absorption lines that would otherwise be present, turning some into emission. We present detailed inferences from the observed absorption spectrum in the subsections below.

In addition to the absorption lines that originate in the (possibly extended) LkH α 225 South photosphere, we also note the presence in our high-resolution optical spectra DIBs. Magakian et al. (2019) also mentioned the presence of DIB features in LkH α 225 South. Specifically, we see 6614, 6379, 5850 (weak), 5797, and 5780 Å DIBs. As mentioned above, these can be used to estimate the extinction to the optical continuum source, as recently done for this source (and others) by Carvalho & Hillenbrand (2022).

6.5.1. Temperature

The low-resolution Palomar/DBSP spectrum (Figure 6) is clearly composite at blue wavelengths. Readily visible are Fe I, Mn I, and Ca I amidst a forest of other absorption lines, including strong Fe II (a hotter line). The high-dispersion spectrum (e.g., Figure 14) allows us to identify additional lines, spectrally resolving them. Many intermediate-excitation neutral

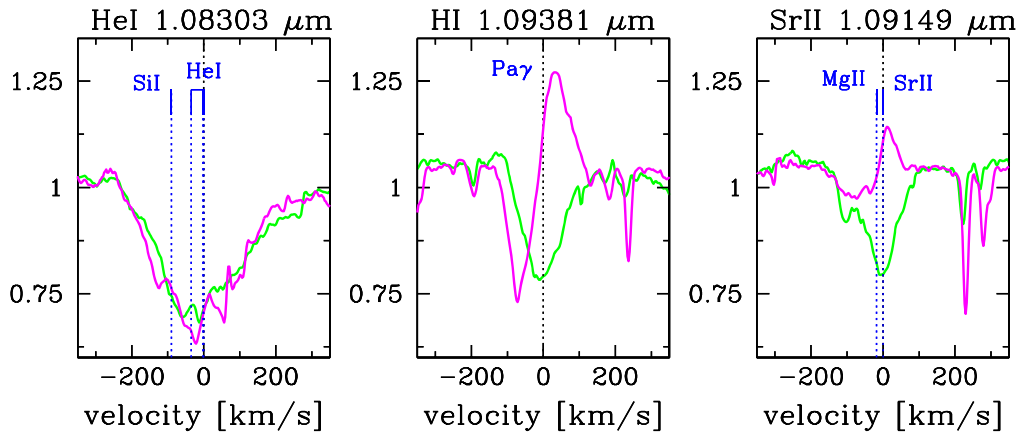


Figure 13. Keck/NIRSPEC line profiles for LkH α 225 South in He I 10830 Å, H I Pa γ , and Sr II. The magenta spectrum is from 2019 June while the green spectrum is from September 2020. In the He I panel, the marked Si I line at 10827 Å is unlikely to be a contributor to the observed profile, given the absence of comparable-strength Si I lines at 10844 and 10870 Å. Similarly, in the Sr II panel, the marked Mg II line at 10914 Å is unlikely to be a contributor to the observed profile, given the absence of a comparable-strength line at 10952 Å. The narrow absorption features in the Pa γ and Sr II panels are uncorrected telluric lines. While the He I profile shows no change, the H I line has evolved from a P Cygni profile to pure absorption. The Sr II profile has evolved similarly. These line profiles can be compared to those exhibited by the cooler optical wind lines of Figure 11.

lines are seen in absorption. Among them are the Fe I 7569 Å (4.3 eV) and Ni I 7573 Å (3.8 eV) featured by Petrov & Herbig (2008). Also present are various Ca I (2.5–3 eV), Mg I (5–6 eV), and Fe II (4–6 eV) lines. The redder range of the spectrum exhibits several even higher excitation lines like Ca II 8912 and 8927 Å (7.1 eV). Perhaps bounding the temperature on the high side, the hot Si II 6347 and 6371 Å (8.1 eV) lines that have been seen in objects like PTF 14jg are not present in LkH α 225 South.

To attempt to discern the approximate temperature of the LkH α 225 South outburst, we compared the dereddened version of the low-resolution optical spectrum to single-temperature standard stars. Based on the strongest metal lines, a best-estimate spectral type across the blue optical is somewhere between a late-F and an early-K star. However, LkH α 225 South is a poor match to any single-temperature template spectrum in this spectral range. The LkH α 225 South spectrum additionally has a pattern of lines that are matched only in mid- and late-A-type stars (appearing much stronger than in the standards) and other lines that are matched only in mid- and late-K-type stars. We thus do not report a spectral type for the outburst spectrum beyond “mixed”.

To assess the spectral type at high dispersion, we perform a cross-correlation analysis of the Keck/HIRES spectrum of LkH α 225 South and a grid of stellar templates selected from the ELODIE spectral library (Prugniel et al. 2007). Figure 15 shows the results of this analysis over three different wavelength ranges, chosen to exclude spectral regions with strongly wind-affected species like those discussed in Section 6.2 above. Based on this analysis, the best spectral type for the photosphere of LkH α 225 South appears to be A3–A6 V. Our quantitative finding can be confirmed by visual examination of the spectra. The pattern of metal absorption lines is well matched to the mid-A spectral type range, with similar strength lines that would be expected in FG spectral type comparison stars not as strongly present.

A further conclusion from the cross-correlation analysis is that there seems to be little evidence for a systematically changing spectral type with wavelength. Although we found evidence in the low-dispersion spectroscopy for a composite spectral type, no clear systematic behavior along these lines is

obvious in the optical high-dispersion data. However, Figure 15 does show that the, e.g., 5200 Å spectral range has a broad plateau of good correlation strength that extends throughout the FG and early-K spectral types. Thus the composite or mixed spectral type conclusion seems robust.

In contrast to the results from single-temperature comparisons, the match of the LkH α 225 South spectrum at blue wavelengths to the FU Ori stars shown in Figure 6 is quite good. The spectrum shows essentially the same detailed absorption pattern exhibited by V2493 Cyg (PTF 10qpf; HBC 722) and V1057 Cyg. The same is true at high dispersion, as shown in Figure 14, which includes the two objects mentioned above as well as V1515 Cyg. Overall, LkH α 225 South appears intermediate between V1515 Cyg and V1057 Cyg in its absorption spectrum, with line widths that are more like the former, and line depths that are more like the latter.

In the infrared, besides the H₂O molecular absorption discussed above, there is little basis on which to estimate a spectral type. The only narrow absorption that is plausibly identified can be associated with the Sr II ion, discussed below as a gravity indicator. Neither hot features, which would be consistent with the early spectral type inferred above from the optical spectrum, nor cool features, such as those which would be consistent with the weak H₂O absorption, are present. The lack of atomic absorption prevents us from quoting an infrared spectral type. Unlike the situation in the blue optical, the infrared spectrum of LkH α 225 South does not appear to be a good match to FU Ori stars (Figure 10).

6.5.2. Gravity Indicators

LkH α 225 South has strong Sr II lines. In the optical, these occur at 4077 and 4216 Å (Figure 6), and in FG stars they indicate low gravity when strong relative to the blueward Fe I 4046, 4063, and 4071 Å or redward Fe I 4271 Å lines. These optical Sr II lines are from multiplet 1. The multiplet 2 infrared Sr II lines at 10328 and 10916 Å (Figures 10, 13) are also present, and also indicative of low gravity. They are prominent in A–M supergiants, moderate in F–M giants, and weak in F–early-K dwarfs (Sharon et al. 2010).

LkH α 225 South also shows Ba II lines. Figure 14 illustrates the 6142 Å line of Ba II in LkH α 225 South. Both this line and

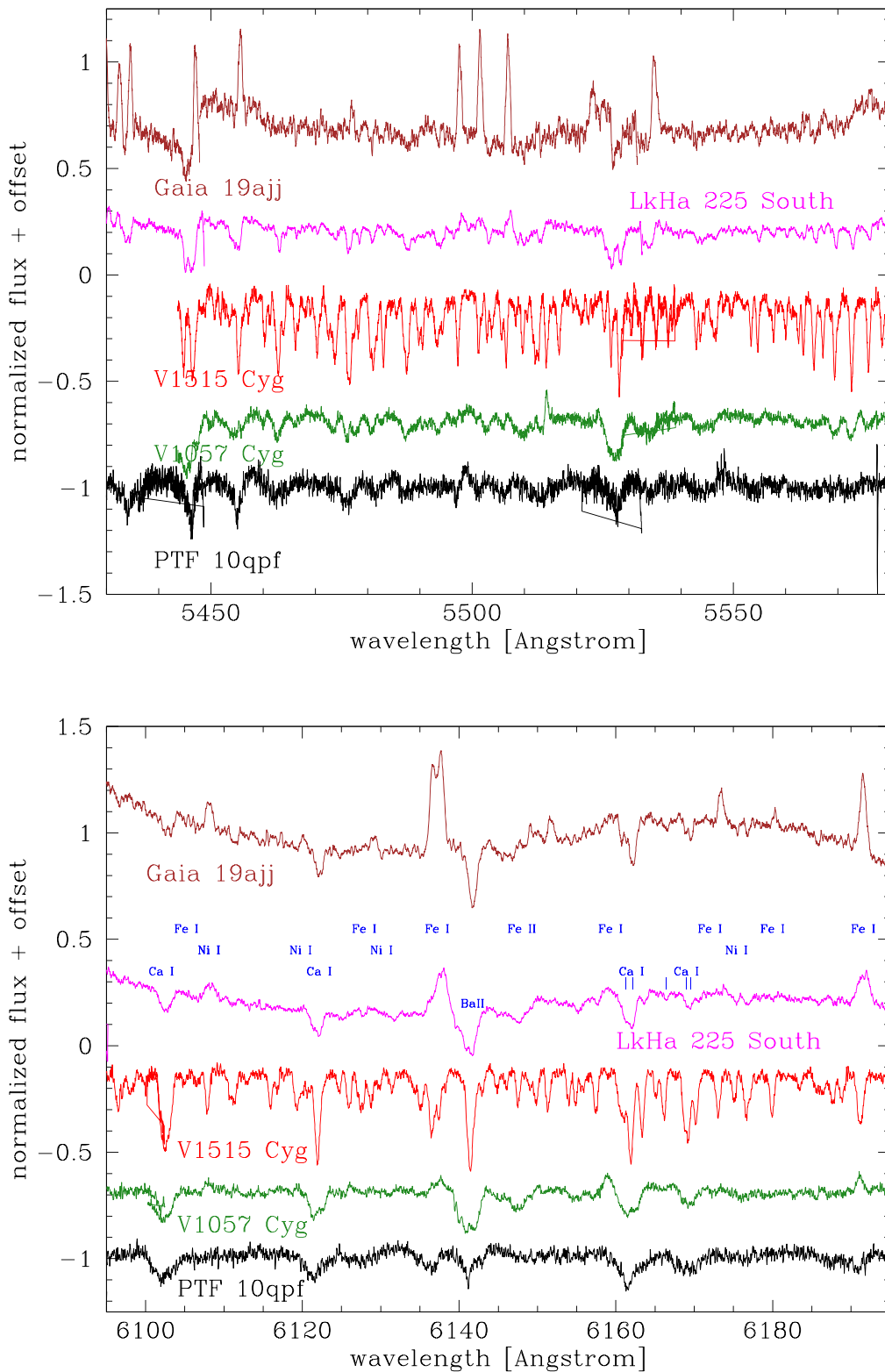


Figure 14. Portions of the 2019 August HIRES spectrum highlighting the spectral similarity of LkH α 225 South (magenta) to other outbursting sources. The absorption component in LkH α 225 South bears resemblance at shorter wavelengths (e.g., top panel) to that of the FU Ori stars V1515 Cyg, V1057 Cyg, and V2493 Cyg (PTF 10qpf, HBC 722). At longer wavelengths (e.g., bottom panel) the absorption component is less obvious, but still present in the stronger lines. Note in particular the presence of Ba II, which is atypical in nonoutbursting T Tauri or Herbig Ae/Be stars, but generally is seen in FU Ori objects. In addition to the weakening absorption component toward longer wavelengths, there is increasingly weak emission, which can be appreciated by comparison with another recent outbursting source, Gaia 19ajj. Like LkH α 225 South, this source has a mixed spectrum of absorption and emission lines in neutral metals, with overall stronger emission and weaker absorption relative to LkH α 225 South.

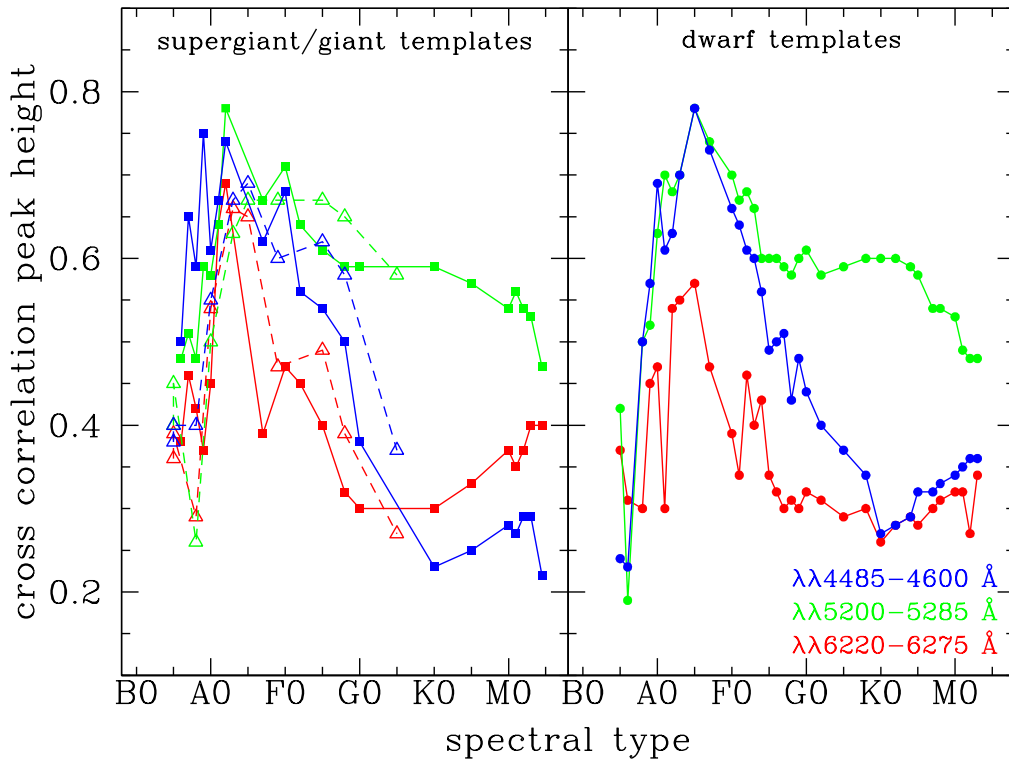


Figure 15. Resulting peak heights from a cross-correlation of LkH α 225 South Keck/HIRES spectrum with a grid of spectral templates from the ELODIE spectral library, plotted as a function of spectral type. Right panel shows dwarf (circles) templates and left panel shows giant (squares) and supergiant (triangles) templates. Blue points are from the 4485–4600 Å region, green 5200–5285 Å, and red 6220–6275 Å. For all wavelength ranges, the best correlations are for stars in the A3–A6 spectral type range, with no clear surface gravity preference. The 5200 Å spectral range has a broad plateau of good correlation strength that extends throughout the FG and early-K spectral types.

the 6497 Å line (not shown) are near-ubiquitously present in FU Ori-type objects, and a signature of a low-gravity atmosphere.

6.5.3. Radial Velocity

We derive a radial velocity for LkH α 225 South from the first Keck/HIRES spectrum of -13.5 ± 0.1 km s $^{-1}$. This is determined using telluric lines as the zero-point reference, as described in Chubak et al. (2012), and the offset from zero velocity of the absorption spectrum. We note that our value is similar to the velocities quoted by Magakian et al. (2019) based on measurements of Fe I and Fe II *emission lines* at lower spectral resolution.

The three Keck/HIRES spectra span a nearly 6 month time period and show no detectable shift in radial velocity, with an upper limit of a few km s $^{-1}$.

6.6. Spectral Changes During 2019

There are perceptible differences in absorption/emission-line strength and morphology among our three Keck/HIRES spectra, taken over about 6 months. The DIBs that are present show no changes, however, giving us confidence in our findings below regarding the small photospheric and wind line differences.

Adopting a period of 43.40 days, as derived above, the three HIRES observations taken at HJD = 2458713.8, 2458816.8, and 2458851.8 span three cadences (see Figure 4). They correspond to phases of 0.43, 0.81, and 0.61, respectively, where phase 0 would be minimum light and phase 0.5 would

be maximum light over the ~ 0.7 mag brightness swing. There is no obvious correlation in the limited data set between spectroscopic behavior occurring closer to phase 0.5 versus that closer to phase 0.0.

The overall trend with time, however, is that the narrow emission lines, which are mainly Fe I, became somewhat weaker. At the same time, absorption lines such as from Fe I, Fe II, and especially Ca I became stronger/deeper. There are also morphology changes in some of the wind lines, with blueshifted absorption components that increased in strength and redshifted emission components that weakened in strength and became narrower. These changes are at the $\sim 10\%$ level in weaker lines, but $>25\%$ in strong emission/absorption features.

Although only [Ca II] was apparent in our first HIRES spectrum, other weaker forbidden lines appeared later. Specifically, weak [O I] 6300 Å and very weak [Fe II] 7155 Å are seen in our second and third HIRES spectra. In the infrared, the SPeX spectrum (Figure 10) taken between the first and second HIRES epochs shows [N I] at 10400 Å, as well as several very weak infrared [Fe I] and perhaps still the [Fe II] 1.25 and 1.644 μ m features. All of these forbidden lines, in addition to others, were seen in Gaia 19ajj (Hillenbrand et al. 2019b).

7. Spectral Energy Distribution Modeling

We model the 0.4–2.4 μ m SED of LkH α 225 South using a Keplerian disk model. A full description of the model and procedure is given in Rodriguez & Hillenbrand (2022), but we briefly summarize here. We adopt a modified Shakura–Sunyaev temperature profile (Kenyon et al. 1988; Zhu et al. 2007), with each annulus radiating as an area-weighted

spectrum given by a NextGen¹⁶ atmosphere (Hauschildt et al. 1999) at the appropriate temperature. The model parameters are as follows. We set the source distance as fixed at $d = 920$ pc, following Magakian et al. (2019), effectively the same as the 916 ± 26 pc argued above based on the parallax of the nearby BD+40° 4124. We assume an inclination $i = 45^\circ$. This value is not well justified, but we were motivated to choose an inclination lower than the $i = 60^\circ$ suggested by a random distribution in $\sin i$, based on the evidence presented in (e.g., Matthews et al. 2007) for an outflow orientation close to pole-on. The outer radius of the disk is fixed at $100 R_\odot$ but varying this parameter has no effect on the overall SED at the wavelengths of interest in this study. The mass of the central star, M_* , radius of the central star, R_* , accretion rate, \dot{M} , and visual extinction, A_V , however, are left as independent free parameters. We also explore joint fitting of $M_*\dot{M}$, since that exercise produces corner plots that are less directly reflective of the prior assumptions.

The SED that we model consists of the low-resolution optical (Palomar/DBSP) and infrared (IRTF/SpEx) spectra, both of which are flux calibrated. Thus, they can be taken together as an accurate SED for the source. As the observations were taken several months apart, the possibility of a flux offset between the optical and infrared SED needs to be considered. The date separation is only two periods (see Figure 4), with just a 5% offset in phase, and no obvious offset in flux; thus we do not include any flux adjustment when fitting the SED. We note that the observations correspond to a phase of the light curve near the minima of the ~ 0.7 mag amplitude oscillations.

To sample the model parameter space and determine which values of the free parameters produce a model that adequately fits the data, we assume Gaussian likelihood and perform a Markov Chain Monte Carlo (MCMC) parameter estimation. We use MCMC to sample the nonanalytic posterior probability distribution that is created once we develop the full accretion-disk model, and have introduced physically reasonable priors for each of our given parameters. The Bayesian nature of MCMC also allows us to marginalize over all parameters except for a single one, and obtain credible intervals which constrain the value of a parameter given our model.

We use the *emcee* package to perform an affine-invariant MCMC routine to sample the parameter space. We explore both a uniform prior and the adoption of a Salpeter initial mass function (IMF) for M_* between $1 M_\odot$ and $15 M_\odot$, a uniform prior on R_* between $0.3 R_\odot$ and $15 R_\odot$, a log-uniform prior on \dot{M} between $10^{-7.5} M_\odot \text{ yr}^{-1}$ and $10^{-3} M_\odot \text{ yr}^{-1}$, and a uniform prior on A_V between 3.0 and 10.0. The log-uniform prior ensures that we sample accretion rates over the many orders of magnitude that are consistent with current FU Ori outburst theories.

We run the MCMC parameter explorations with 16 chains in our affine-invariant sampling, four for each free parameter. We run 6000 steps and take 50% of the steps as the burn-in period. Furthermore, to avoid autocorrelation in our MCMC techniques, we specify steps of 10^{-2} in the appropriate units for each parameter, in addition to our generous burn-in period. After we run our sampler, we test for convergence using the Gelman–Rubin statistic (Vats & Knudson 2018), \hat{R} , and obtain the following values of \hat{R} for the free parameters: M_* : 1.191, R_* : 1.045, \dot{M} : 1.204, A_V : 1.036. The higher values of the statistic for M_* and \dot{M} are to be expected, as these two parameters are strongly correlated in the corner plots and do not

converge to sharply peaked values individually. The \hat{R} values for R_* and A_V , however, are below 1.1. If our MCMC iteration is to converge after infinite iterations, then \hat{R} should converge to 1. We thus set a reasonable standard for \hat{R} , that it be in the range 1.001–1.5 (Vats & Knudson 2018). Adopting a standard for convergence of $\hat{R} = 1.1$, then, allows us to say that the MCMC chains have converged adequately for R_* and A_V .

The resulting values for the four free parameters and their uncertainties are, first for the flat IMF, $M_* = 8.41_{-4.21}^{+4.50} M_\odot$, $R_* = 4.75_{-0.24}^{+0.36} R_\odot$, $\log \dot{M} = -4.48_{-0.19}^{+0.30} \text{ dex } M_\odot \text{ yr}^{-1}$, and $A_V = 7.87_{-0.09}^{+0.06} \text{ mag}$; and, second for the Salpeter IMF, $M_* = 2.75_{-1.50}^{+4.85} M_\odot$, $R_* = 4.69_{-0.25}^{+0.36} R_\odot$, $\log \dot{M} = -4.00_{-0.44}^{+0.34} \text{ dex } M_\odot \text{ yr}^{-1}$, and $A_V = 7.86_{-0.09}^{+0.06} \text{ mag}$. The accompanying corner plots for M_* unfortunately resemble the assumed IMF, rendering this parameter poorly constrained, though it seems clear that M_* must be at least several M_\odot and possibly as high as $\sim 8 M_\odot$. There is strong anticorrelation between M_* and \dot{M} as these two parameters trade off in shifting the SED peak. We further note that the likely more correct Salpeter IMF prior produces a more poorly constrained \dot{M} fit. Joint fitting, however, yields a much tighter constraint in the corner plots, with $\log(M_*\dot{M}) = -3.57_{-0.01}^{+0.01} \text{ dex } M_\odot^2 \text{ yr}^{-1}$. This is consistent with the mean values quoted above for the individual parameters, even though their errors were much higher due to the degeneracy between them.

R_* and A_V each have well-constrained fits in both the four-parameter and three-parameter fitting, from which we conclude that their values are robust to assumptions about the IMF. These two parameters strongly control the overall shape of the SED. Although there is some anticorrelation between R_* and A_V , because A_V modifies the shape of the SED in a different way than R_* , their effects are decoupled by the MCMC parameter exploration, and their values are both meaningfully constrained as a result. The model prediction of an extinction value $A_V = 7.9$ mag is consistent with our estimate based on the dereddening needed to match FGK spectral templates of 4–9 mag, and also the value of 7.2 mag found by Magakian et al. (2019). The model prediction of a moderate mass, as well as a well-constrained radius $R = 4.7 R_\odot$, are consistent with previous indications that LkH α 225 South is an intermediate-mass pre-main-sequence star.

In Figure 16 we show the results from the three-parameter ($M_*\dot{M}$ joint, R_* , and A_V) fitting. The luminosity in the accretion-disk model is $L = 880 L_\odot$, which compares well with the $L = 750 L_\odot$ estimated by Magakian et al. (2019) from bright-state observations. This luminosity is that required from accretion to match the optical/infrared SED, and arises in the innermost $\sim 20 R_*$ of the disk; it does not include energy reradiated by the substantial amount of circumstellar dust in this source. The maximum temperature in the accretion-disk model is $T_{\text{max}} = 9400$ K.

8. Discussion

Our discussion is centered around three aspects of LkH α 225 South: the current bright-state quasiperiodicity, the presentation of a mixed-temperature absorption spectrum, and the overall interpretation and context of this source in the panoply of young-stellar-object outbursts.

8.1. Interpretation of the Quasiperiodicity Near Peak

Periodicities in astrophysical sources usually find explanation in terms of some form of rotational, orbital, or pulsational

¹⁶ BT-NextGen (AGSS 2009) available at <http://svo2.cab.inta-csic.es/theory/newov2/>.

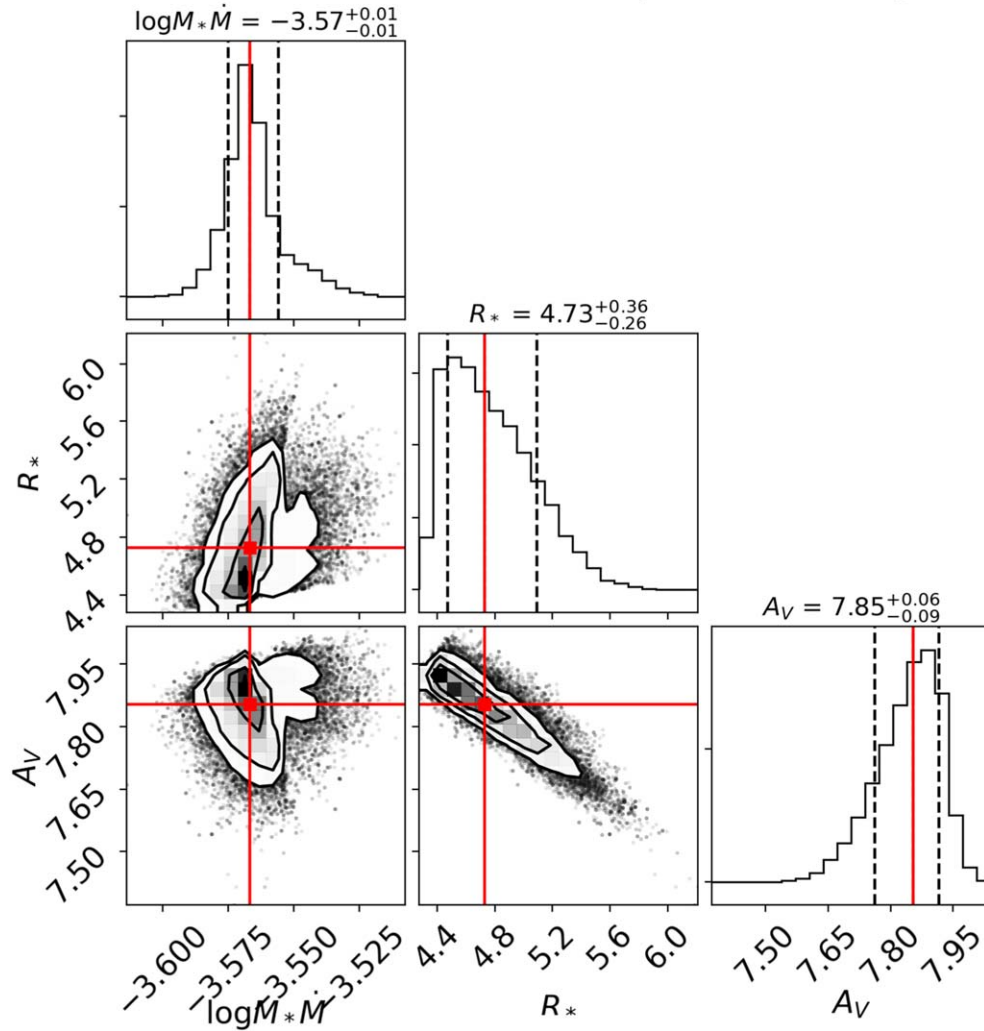
LH α 225s MCMC Corner Plot: Optical + NIR Spectra

Figure 16. “Corner plot” output from the Markov Chain Monte Carlo fitting procedure applied to the spectral energy distribution of LkH α 225 South that is shown in Figure 5. The preferred parameter values are given above the boxes and shown as red lines, with formal uncertainties indicated as vertical dashed lines. The units in the panels are $M_{\odot}^2 \text{ yr}^{-1}$, R_{\odot} , and magnitudes, along the diagonal.

behavior. In the case of LkH α 225 South, there is no clear explanation.

The observed oscillatory behavior in LkH α 225 South near its light-curve peak is nonsinusoidal but colorless. While the g and r magnitudes undergo ~ 0.7 mag periodic changes, the $g - r$ color does not vary significantly. We know that the oscillations are occurring now, and likely have been for the past 6 + yr of the current brightness maximum of LkH α 225 South—given that Magakian et al. (2019) also reported colorless variability, and their photometry lines up fairly well with our phased light curve; see Figure 8. However, there is no evidence that such oscillations were not occurring previously, in the data from earlier decades. One line of evidence against this is that, in contrast to the recent colorless oscillatory behavior, Herbst & Shevchenko (1999) demonstrated a color–magnitude trend in the brightness fluctuations of LkH α 225 South, when it was around 15^m , and color changes in $V - R$ of $\sim 3.5^m$ accompanying the brightness drop of $\sim 4^m$.

We can consider the observed large-amplitude periodicity of LkH α 225 South relative to similar periodicities that have been detected in other young stellar objects. These seem to fall into

two categories.¹⁷ One features regular fluctuations of 0.5–2 mag that are consistent over years to decades, and appear to

¹⁷ Another set of accretion-outburst sources with claimed low-amplitude periodicities are FU Ori, V2493 Cyg, and ASAS 13db. In these objects, the evidence for truly periodic behavior—as opposed to mere “timescales” for change—seems somewhat weak. In FU Ori, short-timescale (sub-day) variations were reported by Kenyon et al. (2000) as nonperiodic “flickering” at the few percent level, and associated with the dynamical time at the inner edge of an accretion disk surrounding a $1 M_{\odot}$, $4 R_{\odot}$ central source (in analogy to cataclysmic variable and X-ray binary systems). Errico et al. (2003), Herbig et al. (2003), and Powell et al. (2012) all detected quasiperiodicities in line profiles of FU Ori, one at ~ 13 – 15 days associated with the wind, and one at ~ 3.5 days associated with the disk. Siwak et al. (2018) used high-precision photometry from the Microvariability and Oscillations of Stars satellite to confirm photometric variations on approximately these same two timescales, finding quasiperiodic signals at ~ 10 – 11 and ~ 1.5 – 3 days. Green et al. (2013) discussed a potential quasiperiodicity for V2493 Cyg (also known as PTF 10qpf and, in the pre-outburst stage, as HBC 722 or LkH α 188/G4), another FU Ori-type object. Two timescales were also found for this object, 5.8 and 1.3 days. However, the phasing is not convincing, and the findings have not been independently confirmed. Finally, Sicilia-Aguilar et al. (2017) argue for a ~ 4 day periodicity in the outburst phases of ASAS 13db, an EX Lup-type star, which they link to the rotation period of the star and attribute to the circulation of a new hot spot associated with the enhanced accretion event. Again, the phased light curves are not particularly compelling, however.

indicate a cyclic manner of accretion from a disk on to the central star. The other manifests only after a large-amplitude brightness increase, and appears as fluctuations superposed on top of a dominant, long-term accretion outburst.

V371 Ser (Hodapp et al. 2012; Lee et al. 2020), V2492 Cyg (Covey et al. 2011; Hillenbrand et al. 2013), and V347 Aur (Dahm & Hillenbrand 2020) all exhibit long-timescale (months to >1 yr) quasiperiodicities accompanied by color variations that have lasted for perhaps decades. The authors of the cited papers appeal to some sort of cycling in the inner disk, perhaps driven by an unseen companion, as explanation for the observations. In these sources, there is a seemingly regular change between low-state and high-state accretion, as evidenced by time-series spectroscopy or color-magnitude behavior. These sources are distinct from EX Lup-type objects, in that their brightenings are more regular, as opposed to more randomly timed, with light-curve shapes that are more rounded at their peaks as opposed to the top-hat-like peaks that characterize, e.g., EX Lup and V1647 Ori.

More similar to the case of LkH α 225 South than the above regularly varying accretors are sources like L1634 IRS7 and ESO H α -99. These have both shown brightness quasiperiodicity following a clearly detected, long-timescale, large-amplitude outburst. Hodapp & Chini (2015) demonstrated L1634 IRS7 to have a remarkable ~ 2 mag amplitude at the K_s band, with a 37 day periodic signal that is superposed on a slow rise over about two decades. Hodapp et al. (2019) classified ESO H α -99 as an EX Lup-type star, but one that exhibits ≈ 0.5 mag amplitude variations on timescales of about a month, with a semiperiodic morphology. Again, the behavior is superposed on a brightness plateau that followed a 4.4 mag brightening over about a year. The ESO H α -99 brightness oscillations are interpreted in terms of a rotating structure within the circumstellar disk, an explanation we also explore for the situation of LkH α 225 South.

Like L1634 IRS7 and ESO H α -99, LkH α 225 South has a quasiperiodic light-curve morphology during its light-curve plateau, and the amplitudes are also comparable at about a factor of two fluctuations. However, LkH α 225 South has experienced a much larger amplitude overall brightening (>7 mag), on a significantly longer timescale (~ 15 yr). If orbital in origin, the 43 day period in LkH α 225 South would correspond to changes in brightness occurring on a size scale of $\sim 0.49 \times (M/8.4 M_\odot)$ au. This is still inside the outbursting disk according to our disk model (Section 7), in a region where the temperature of the disk is ≈ 1750 K.

The temperature range is interesting because it corresponds to the approximate temperature where the TiO and VO molecules that we observe start to exist ($1500 \lesssim T \lesssim 4000$ K). It is also consistent with the dust-destruction temperature ($T \gtrsim 1200$ – 1800 K), and thus could coincide with a region where the hot disk is cool enough to also have dust. The periodicity, if driven by orbital phenomena, may be related to turbulence or to azimuthally asymmetric phenomena occurring at this special location. However, the periodic variability we observe is in the optical (g and r bands). Here, the disk is expected to be much hotter than the relevant ≈ 1750 K. Specifically, the photons dominating the flux at these wavelengths are coming from ≈ 7000 – 7400 K regions in our disk model. It is unclear what in this temperature range could be varying on the observed 43 day timescale.

In the simulations of Zhu et al. (2009), a gravitational instability somewhat further out in the disk causes matter to rush inward, triggering a magnetorotational instability, which in turn triggers a thermal instability in the innermost disk. The temperature at which the magnetorotational instability begins to take effect is ~ 1200 K, somewhat lower than the ≈ 1750 K estimate above. Lower temperatures are possible for outburst-accretion rates that are lower than the fiducial model of $10^{-4} M_\odot \text{ yr}^{-1}$.

An alternative to being a special place in the disk, as argued above, is that the periodic variability near maximum brightness for LkH α 225 South is related to an orbiting companion that affects the disk brightness quasiperiodically, on its orbital timescale. As above, given our estimate of M_* and the inferred period, the purported companion would be located at 0.49–0.62 au, depending on the mass ratio. The current bright state yields no evidence in photometry or radial velocities for a binary companion. However, if the period is associated with an unseen companion located within the disk-instability region, that companion might be acting as a gatekeeper for accretion from the outer disk, causing quasiperiodic modulation of the accretion by a factor of two (0.7 mag). It is unclear whether the profile of the light curve (Figure 8) is consistent with such a scenario, however.

Another possibility is some sort of slow pulsational behavior. One scenario is pulsational ringing following a planet engulfment. In order to produce a period of 43 days, however, the star would have to have swelled to $230 R_\odot$, which is ~ 1.5 dex larger than the size inferred from our SED modeling, and therefore seems unlikely. Another pulsational scenario is that of acoustic-mode trapping in the disk-to-star boundary layer and the inner disk, studied by Belyaev et al. (2012). Both the amplitudes and periods are much smaller (Coleman et al. 2022) than in our case, however.

8.2. Interpretation of The Mixed Absorption Spectrum

Summarizing the inferences that can be made from the object’s spectrum, we have found evidence for a mid-A spectral type from the high-resolution optical spectrum, an FGK spectral type from the low-resolution optical spectrum, and also absorption from much cooler H $_2$ O molecules in the infrared spectrum, as might characterize an M spectral type. At a minimum, we can conclude that the spectral type is mixed, or composite. We further offer the hypothesis that what we may be seeing in this source is a disk spectrum, but with a warm wind that gives rise to the hotter spectral type inferred from the optical metal lines in the high-dispersion data.

We developed the disk hypothesis in more detail in Section 7 by fitting the optical to near-infrared SED. The stellar mass derived from the disk modeling is several M_\odot and possibly as high as $\sim 8 M_\odot$, which would correspond to a spectral type later than B2 on the main sequence, and temperature $< 20,500$ K. The maximum temperature in the innermost disk annulus is 9400 K in the model, which would correspond to a spectral type of A1. Rather than seeing the hottest parts of the disk directly, the spectral type we estimate from the optical high-dispersion spectrum seems dominated by a component that is a bit later, $\sim A3$ – $A6$.

The seemingly disparate pieces of information above are consistent with one another in the scenario where an embedded young star has undergone an outburst and is now presenting a disk-dominated spectrum. In addition to the evidence for a

mixed or composite absorption spectrum, we have reported that the absorption lines in LkH α 225 South have the narrow width of V1515 Cyg (supporting a low inclination), but the relatively shallow depth of V1057 Cyg (supporting significant disk broadening). A comparison to FU Ori itself also shows good agreement, with the exception of the lower-excitation lines, which are in absorption in FU Ori but in emission in LkH α 225 South.

8.3. What is this Source?

LkH α 225 South has brightened by >7 mag over the past two decades, seemingly without much change in its optical color, but a clear blueing of the near-infrared SED. The color changes imply that extinction clearing is not a dominant factor in the brightening. Instead, the behavior is more consistently explained by the effects of enhanced accretion, or a combination of enhanced accretion and extinction clearing.

Connelley & Reipurth (2018) state, based on the archetypal examples of FU Ori, V1057 Cyg, and V1515 Cyg, that FU Ori stars are spectroscopically defined as having (in infrared spectra) “strong CO absorption, weak metal absorption, strong water bands, low gravity, strong blueshifted He I absorption, and few (if any) emission lines”. By this definition, LkH α 225 South does not qualify as an FU Ori star. Yet it does have FU Ori–like absorption in the blue optical (Figures 6, 14), though without much indication of a systematic spectral type dependence on wavelength (Figure 15). Instead, the dominant spectral class is fairly consistent across wavelengths at \sim mid-A, though there is also reasonable correlation in some parts of the spectrum with cooler FG and early-K temperatures, and in the infrared, with M-type temperatures. The source also has low-gravity signatures in the form of Sr II and Ba II lines.

The weak emission-line spectrum of LkH α 225 South is similar to, but more muted than, that of other outbursting young stars such as Gaia 19ajj, V2492 Cyg (PTF 10nvg), and V1647 Ori. Gaia 19ajj has only atomic emission, which is slightly stronger than what is seen in LkH α 225 South. V2492 Cyg has similar atomic but also the molecular emission in TiO/VO and CO that is seen in LkH α 225 South; it differs from LkH α 225 South in having H $_2$ O emission, which is in absorption in LkH α 225 South (as well as in Gaia 19ajj). Both V2492 Cyg (PTF 10nvg) and V1647 Ori have stronger emission lines and much less of an absorption signature than seen in the mixed-temperature spectrum of LkH α 225 South.

We support the conclusion of Magakian et al. (2019) that there is a strong wind in the outburst state of LkH α 225 South (Figures 11, 13). The relatively low wind velocity, only about -150 km s $^{-1}$, suggests a low to modest inclination for the source. A low inclination is also supported by the narrow absorption line widths in the optical. Further, the shape of the CO bandhead lines lacks the morphology expected (Martin 1997) from a highly inclined source.

Overall, LkH α 225 South in outburst seems a lot like Gaia 19ajj, sharing many of the properties described above. Both sources have evidence for large-amplitude optical outbursts, taking years to more than a decade to develop, and previous bright photometric states, with potential repeat timescales of one to a few decades. LkH α 225 South has a stronger absorption spectrum, which is more similar to those in the FU Ori stars at the bluest wavelengths. It also has TiO emission, which was not seen in Gaia 19ajj, as well as stronger CO emission. LkH α 225 South has a weaker emission spectrum

than Gaia 19ajj, which is present only at red optical and near-infrared wavelengths.

A further interesting aspect of LkH α 225 South is its mass, which is likely in the range of several to $\sim 8 M_{\odot}$. As such, while not massive, it certainly qualifies as an intermediate-mass young star undergoing accretion-driven outburst behavior.

9. Conclusions

We have reported on a detailed study of the spectroscopic and photometric presentation of LkH α 225 South during its current bright state. Our study adds to the work of Magakian et al. (2019), who first reported the dramatic brightening of this enigmatic young stellar object. LkH α 225 South was visible in the 1950s (POSS-I plates), but not in the early 1980s (Quick-V plates). It was recorded as moderately bright in the late 1980s (Shevchenko et al. 1993), then faded by the 1990s (POSS-II plates; Hillenbrand et al. 1995; Herbst & Shevchenko 1999). It appears to have started brightening again in the late 2000s, reaching something of a plateau in ~ 2015 .

Our main new findings regarding LkH α 225 South are as follows.

1. A nonsinusoidal, colorless, quasiperiodic light curve in the bright state. While the phased light curve has significant dispersion, the oscillations have persisted for over 3 yr. The derived period is ~ 43 days and the amplitude ~ 0.7 mag.
2. A currently decreasing emission spectrum and increasing absorption spectrum, based on limited spectral time-series data as the outburst continues to develop in its long plateau phase.
3. Absorption features at blue optical wavelengths and in the near-infrared which indicate a mixed-temperature photosphere having mid-A to M-type absorption components present. The spectrum can not be characterized with a single spectral type in the traditional sense. Low gravity is evidenced by the strength of the Sr II and Ba II lines.
4. Strong wind signatures in H α , He I 10830 Å, and a variety of metal lines including Ca II doublet and triplet, Fe II, Na I D, K I, Mg Ib, O I triplet, and Li I.
5. Atomic emission lines that are strongest in the red optical and short-wavelength infrared, dominating the spectrum at these wavelengths, but essentially absent at blue optical wavelengths.
6. Molecular emission from TiO and CO both before and after the brightening, with no evidence for line-to-continuum change. Molecular emission from H $_2$ that, relative to the continuum, weakened after the brightening.
7. Molecular absorption by H $_2$ O that was enhanced after the brightening.
8. As the star brightened, a decrease in the steep spectral slope, or blueing behavior corresponding to a reduction in extinction by $A_V \approx 3$ mag. We find a current extinction value of $A_V \approx 8$ mag.
9. Stellar parameters M_{*} = several to $8 M_{\odot}$ and R_{*} = $4.7 R_{\odot}$, and an accretion rate $\log \dot{M} = -4.5$ to -4 dex $M_{\odot} \text{ yr}^{-1}$ result from an accretion-disk model fit to flux-calibrated spectrophotometry. The corresponding luminosity in the accretion-disk model is $L = 880 L_{\odot}$.
10. Evidence for a relatively low source inclination, based on (disk-broadened) absorption line widths, CO bandhead

emission profiles, and P Cygni profile terminal velocities, consistent with inferences in previous literature.

LkH α 225 South deserves further study, but the current best interpretation is that the source has undergone a long-timescale accretion outburst, perhaps related to an orbiting companion at ≈ 0.49 au. Phenomenologically, the source bears some resemblance to FU Ori stars in the blue wavelengths, with a mixed-temperature, pure-absorption absorption spectrum. LkH α 225 South is not entirely FU Ori–like, though, considering the weak low-excitation metal emission and the lack of strong molecular absorption in the near-infrared. It is like PTF 14jg in this regard, though not as hot.

The large-amplitude, very-long-timescale photometric variations of LkH α 225 South are like those of sources such as PV Cep, V2492 Cyg (PTF 10nvg), and Gaia 19ajj. However, while these sources share aspects of their emission-line spectra at red optical and near-infrared wavelengths (which are even stronger than in LkH α 225 South), they do not have prominent absorption spectra like LkH α 225 South does. The quasiperiodicity of LkH α 225 South near its current light-curve peak is reminiscent of the infrared sources L1634 IRS7 and ESO H α -99, which are also similar in exhibiting near-infrared CO emission.

We acknowledge the work of former Caltech undergraduate Sirin Caliskan, who produced the photometry and astrometry for the Keck/LRIS images. We acknowledge with thanks the AAVSO International Database, which allowed us to connect with coauthor D.R.P. We thank Roc Cutri for consultation regarding whether the saturated photometry of LkH α 225 South could be recovered in NEOWISE data. We thank Kishaley De for checking on the source in Gattini data. Andrew Howard facilitated the first Keck/HIRES spectrum. Erik Petigura and Trevor David kindly obtained the first Keck/NIRSPEC data set; Jessica Spake kindly allowed for the second. We thank Richard Larson for his interest in this system, and for his suggestions regarding the 43 day quasiperiodicity. We also thank the referee for a careful and insightful review of our work.

Facilities: IPHaS, PanSTARRS, AAVSO, Gaia, PO: 1.2m (PTF), PO: 1.2m (ZTF), IRSA, ASAS, PO: Hale (DBSP), Keck:I (HIRES), Keck:II (NIRSPEC), IRTF (SpeX), Gemini (NIRI).

ORCID iDs

Howard Isaacson  <https://orcid.org/0000-0002-0531-1073>

Antonio C. Rodriguez  <https://orcid.org/0000-0003-4189-9668>

Michael Connelley  <https://orcid.org/0000-0002-8293-1428>

Bo Reipurth  <https://orcid.org/0000-0001-8174-1932>

Michael A. Kuhn  <https://orcid.org/0000-0002-0631-7514>

Tracy Beck  <https://orcid.org/0000-0002-6881-0574>

References

Andrillat, Y., & Swings, J. P. 1976, *ApJL*, 204, L123
 Aspin, C., Sandell, G., & Weintraub, D. A. 1994, *A&A*, 282, L25
 Bae, J.-H., Kim, K.-T., Youn, S.-Y., et al. 2011, *ApJS*, 196, 21
 Barentsen, G., Vink, J. S., Drew, J. E., & Sale, S. E. 2013, *MNRAS*, 429, 1981
 Bautista, M. A., Fivet, V., Ballance, C., et al. 2015, *ApJ*, 808, 174
 Bellm, E. C., Kulkarni, S. R., Graham, M. J., et al. 2019, *PASP*, 131, 018002
 Belyaev, M. A., Rafikov, R. R., & Stone, J. M. 2012, *ApJ*, 760, 22

Carvalho, A., & Hillenbrand, L. A. 2022, *AJ*, submitted
 Chubak, C., Marcy, G., Fischer, D. A., et al. 2012, arXiv:1207.6212
 Coleman, M. S. B., Rafikov, R. R., & Philippov, A. A. 2022, *MNRAS*, 509, 440
 Connelley, M. S., & Reipurth, B. 2018, *ApJ*, 861, A145
 Covey, K. R., Hillenbrand, L. A., Miller, A. A., et al. 2011, *AJ*, 141, 40
 Cutri, R. M., Mainzer, A., Conrow, T., et al. 2015, Explanatory Supplement to the NEOWISE Data Release Products, <http://wise2.ipac.caltech.edu/docs/release/neowise/expsup>
 Cutri, R. M., Wright, E. L., Conrow, T., et al. 2012, Explanatory Supplement to the WISE All-Sky Data Release Products
 Dahm, S. E., & Hillenbrand, L. A. 2020, *AJ*, 160, 278
 De, K., Hankins, M. J., Kasliwal, M. M., et al. 2020, *PASP*, 132, 025001
 Errico, L., Vittone, A., & Lamzin, S. A. 2003, *AstL*, 29, 105
 Fitzpatrick, E. L. 1999, *PASP*, 111, 63
 Flewelling, H. A., Magnier, E. A., Chambers, K. C., et al. 2020, *ApJS*, 251, 7
 Gaia Collaboration, Brown, A. G. A., Vallenari, A., et al. 2018, *A&A*, 616, A1
 Graham, M. J., Kulkarni, S. R., Bellm, E. C., et al. 2019, *PASP*, 131, 078001
 Green, J. D., Robertson, P., Baek, G., et al. 2013, *ApJ*, 764, 22
 Gutermuth, R. A., Megeath, S. T., Myers, P. C., et al. 2009, *ApJS*, 184, 18
 Hankins, M., Hillenbrand, L. A., De, K., et al. 2020, *ATel*, 13902
 Hauschildt, P. H., Allard, F., Ferguson, J., et al. 1999, *ApJ*, 525, 871
 Herbig, G. H. 1960, *ApJS*, 4, 337
 Herbig, G. H., Petrov, P. P., & Duemmler, R. 2003, *ApJ*, 595, 384
 Herbst, W., & Shevchenko, V. S. 1999, *AJ*, 118, 1043
 Herczeg, G. J., & Hillenbrand, L. A. 2014, *ApJ*, 786, 97
 Hillenbrand, L. A., Contreras Peña, C., Morrell, S., et al. 2018, *ApJ*, 869, 146
 Hillenbrand, L. A., Knapp, G. R., Padgett, D. L., et al. 2012, *AJ*, 143, 37
 Hillenbrand, L. A., Meyer, M. R., Strom, S. E., et al. 1995, *AJ*, 109, 280
 Hillenbrand, L. A., Miller, A. A., Carpenter, J. M., et al. 2019a, *ApJ*, 874, 82
 Hillenbrand, L. A., Miller, A. A., Covey, K. R., et al. 2013, *AJ*, 145, 59
 Hillenbrand, L. A., Reipurth, B., Connelley, M., et al. 2019b, *AJ*, 158, 240
 Hodapp, K. W., & Chini, R. 2015, *ApJ*, 813, 107
 Hodapp, K. W., Chini, R., Watermann, R., & Lemke, R. 2012, *ApJ*, 744, 56
 Hodapp, K. W., Reipurth, B., Pettersson, B., et al. 2019, *AJ*, 158, 241
 Howard, A. W., Johnson, J. A., Marcy, G. W., et al. 2010, *ApJ*, 721, 1467
 Ibragimov, M. A., Mel'nikov, S. Y., Chernyshov, A. V., et al. 1988, *Afz*, 29, 633
 Jordi, K., Grebel, E. K., & Ammon, K. 2006, *A&A*, 460, 339
 Kenyon, S. J., Hartmann, L., & Hewett, R. 1988, *ApJ*, 325, 231
 Kenyon, S. J., Kolotilov, E. A., Ibragimov, M. A., et al. 2000, *ApJ*, 531, 1028
 Lee, S., Lee, J.-E., Aikawa, Y., Herczeg, G., & Johnstone, D. 2020, *ApJ*, 889, 20
 Looney, L. W., Wang, S., Hamidouche, M., et al. 2006, *ApJ*, 642, 330
 Magakian, T. Y., & Movsessian, T. A. 1997, *AstL*, 23, 666
 Magakian, T. Y., Movsessian, T. A., Andreasyan, H. R., et al. 2019, *A&A*, 625, A13
 Martin, E. C., Fitzgerald, M. P., McLean, I. S., et al. 2018, *Proc. SPIE*, 10702, 107020A
 Martin, S. C. 1997, *ApJL*, 478, L33
 Marvel, K. B. 2005, *AJ*, 130, 2732
 Masci, F. J., Laher, R. R., Rusholme, B., et al. 2019, *PASP*, 131, 018003
 Matthews, B. C., Graham, J. R., Perrin, M. D., et al. 2007, *ApJ*, 671, 483
 McLean, I. S., Becklin, E. E., Bendiksen, O., et al. 1998, *Proc. SPIE*, 3354, 566
 Miller, A. A., Hillenbrand, L. A., Bilgi, P., et al. 2015, *ATel*, 7428
 Mora, A., Merín, B., Solano, E., et al. 2001, *A&A*, 378, 116
 Navarete, F., Damineli, A., Barbosa, C. L., et al. 2015, *MNRAS*, 450, 4364
 Oke, J. B., Cohen, J. G., Carr, M., et al. 1995, *PASP*, 107, 375
 Oke, J. B., & Gunn, J. E. 1982, *PASP*, 94, 586
 Palla, F., Testi, L., Hunter, T. R., et al. 1995, *A&A*, 293, 521
 Pecchioli, T., Sanna, N., Massi, F., et al. 2016, *PASP*, 128, 073001
 Petrov, P. P., & Herbig, G. H. 2008, *AJ*, 136, 676
 Powell, S. L., Irwin, M., Bouvier, J., et al. 2012, *MNRAS*, 426, 3315
 Prugniel, P., Soubiran, C., Koleva, M., et al. 2007, arXiv:0703658
 Purser, S. J. D., Lumsden, S. L., Hoare, M. G., et al. 2021, *MNRAS*, 504, 338
 Rayner, J. T., Toomey, D. W., Onaka, P. M., et al. 2003, *PASP*, 115, 362
 Rodriguez, A. C., & Hillenbrand, L. A. 2022, arXiv:2112.01549
 Sandell, G., Wiesemeyer, H., Requena-Torres, M. A., et al. 2012, *A&A*, 542, L14
 Shappee, B., Prieto, J., Stanek, K. Z., et al. 2014, AAS Meeting, 223, 236.03
 Sharon, C., Hillenbrand, L., Fischer, W., & Edwards, S. 2010, *AJ*, 139, 646
 Shevchenko, V. S., Grankin, K. N., Ibragimov, M. A., et al. 1993, *Ap&SS*, 202, 121
 Sicilia-Aguilar, A., Oprandi, A., Froebrich, D., et al. 2017, *A&A*, 607, A127
 Siwak, M., Winiarski, M., Ogłozza, W., et al. 2018, *A&A*, 618, A79
 Strom, K. M., Strom, S. E., Breger, M., et al. 1972, *ApJL*, 173, L65

- Terranegra, L., Chavarría-K, C., Diaz, S., et al. 1994, *A&AS*, **104**, 557
- van den Ancker, M. E., Wesselius, P. R., & Tielens, A. G. G. M. 2000, *A&A*, **355**, 194
- VanderPlas, J. T. 2018, *ApJS*, **236**, 16
- Vats, D., & Knudson, C. 2018, arXiv:1812.09384
- Vogt, S. S., Allen, S. L., Bigelow, B. C., et al. 1994, *Proc. SPIE*, **2198**, 362
- Wenzel, W. 1972, *IBVS*, **713**, 1
- Zhu, Z., Hartmann, L., Calvet, N., et al. 2007, *ApJ*, **669**, 483
- Zhu, Z., Hartmann, L., Gammie, C., & McKinney, J. C. 2009, *ApJ*, **701**, 620
- Zhu, Z., Jiang, Y.-F., & Stone, J. M. 2020, *MNRAS*, **495**, 3494